THE ASTROPHYSICAL JOURNAL SUPPLEMENT SERIES, 129:247–266, 2000 July

HIGH-RESOLUTION ELECTRON-IMPACT EMISSION SPECTRUM OF H_2. I. CROSS SECTIONS AND EMISSION YIELDS 900–1200 Å

C. JONIN[1,2]
Jet Propulsion Laboratory, California Institute of Technology, Pasadena, CA 91109
XIANMING LIU
Department of Aerospace and Mechanical Engineering, University of Southern California, Los Angeles, CA 90089
J. M. AJELLO AND G. K. JAMES
Jet Propulsion Laboratory, California Institute of Technology, Pasadena, CA 91109
AND
H. ABGRALL
Observatoire de Paris, Section de Meudon, DAEC; and CNRS UMR 8631, 92195 Meudon Cedex, France
Received 1999 December 9; accepted 2000 January 27

ABSTRACT

High-resolution ($\Delta\lambda = 115$ mÅ) emission spectra of molecular hydrogen produced by electron-impact excitation at 100 eV have been obtained in the wavelength range 900–1200 Å. The emission spectra can be assigned to transitions between the $X\ ^1\Sigma_g^+$ ground state and the $1s\sigma_g np\sigma_u\ ^1\Sigma_u$ and $1s\sigma_g np\pi_u\ ^1\Pi_u$ Rydberg states. Synthetic rotational line spectra based on the excitation function of Liu et al. and calculated $2p\sigma\ B\ ^1\Sigma_u^+$–$X\ ^1\Sigma_g^+$, $2p\pi\ C\ ^1\Pi_u$–$X\ ^1\Sigma_g^+$, $3p\sigma\ B'\ ^1\Sigma_u^+$–$X\ ^1\Sigma_g^+$, and $3p\pi D\ ^1\Pi_u$–$X\ ^1\Sigma_g^+$ transition probabilities of Abgrall et al. are generally found to be in good agreement with the experimental spectra in the regions where emissions from $1s\sigma_g np\sigma_u$ ($n \geq 4$) and $1s\sigma_g np\pi_u$ ($n \geq 4$) states are negligible. Emission cross sections for $D\ ^1\Pi_u^+$, $D'\ ^1\Pi_u$, and $D''\ ^1\Pi_u^-$, $B'\ ^1\Sigma_u^+$, and $B''\ ^1\Sigma_u^+$ states are obtained by measuring the emission intensities from these states relative to those from the $B\ ^1\Sigma_u^+$, $C\ ^1\Pi_u$, and $D\ ^1\Pi_u^-$ states. A high- resolution EUV calibration technique is established. At 100 eV the emission cross sections of the $D\ ^1\Pi_u$, $D'\ ^1\Pi_u$, $D''\ ^1\Pi_u$, $B'\ ^1\Sigma_u^+$, and $B''\ ^1\Sigma_u^+$ states are measured to be $(2.8 \pm 0.4) \times 10^{-18}$, $(6.3 \pm 1.3) \times 10^{-19}$, $(5.9 \pm 1.7) \times 10^{-20}$, $(2.1 \pm 0.3) \times 10^{-18}$, and $(1.6 \pm 0.4) \times 10^{-19}$ cm^2, respectively. In addition, the vibrational emission cross sections have been compared to the estimated excitation cross sections to obtain the predissociation yields for selected vibrational levels of the $D\ ^1\Pi_u^+$, $D'\ ^1\Pi_u^+$ and $D''\ ^1\Pi_u^+$ states. The $B'\ ^1\Sigma_u^+$ state is inferred to have very significant excitation into the H(1*s*) + H(2*p*, 2*s*) dissociative continuum.

Subject headings: methods: laboratory — molecular processes — ultraviolet: ISM

1. INTRODUCTION

Electron-impact excitation of molecular hydrogen is an important astrophysical process. Since the early *Voyager* and *IUE* flights, it has been known that electron-impact excitation of H_2 is the primary VUV emission process in the atmospheres of outer planets (Broadfoot et al. 1979; Clarke et al. 1980). Several recent spacecraft observations of Jupiter aurorae with the *Hubble Space Telescope* (Clarke et al. 1994; Trafton et al. 1994; and Kim, Caldwell, & Fox 1995) and with the *Galileo* spacecraft (Ajello et al. 1998) have all confirmed the importance of electron-impact excitation of H_2. In addition, collisional excitation of H_2 has been observed by the Hopkins Ultraviolet Telescope (HUT) at low resolution in the extreme ultraviolet (EUV) region from the outer planets (Morrissey et al. 1997) as well as from Herbig-Haro objects in the interstellar medium (ISM) (Raymond, Blair, & Long 1997). The *Cassini* spacecraft en route to Saturn is equipped with a UV spectrometer to study H_2 aurorae in both the EUV (800–1150 Å) and far-ultraviolet (FUV) (1150–1700 Å) regions. Finally, the recent launch of the *Far Ultraviolet Spectroscopic Explorer* (*FUSE*) satellite observatory with a resolving power ($\lambda/\Delta\lambda$) of 30,000 and spectral range from 905 to 1187 Å, which has included many guaranteed observation time for the outer planets and ISM, attests the continued keen interest in high-resolution emission studies of H_2 in the EUV region.

Electron-impact excitation of H_2 is a significant process in certain dense interstellar clouds by a variety of mechanisms. First, cosmic-ray radiation produces a large number of electrons (Cravens & Dalgarno 1978; Sternberg, Dalgarno, & Lepp 1987; Gredel et al. 1989). When molecular clouds are irradiated with intense, penetrating X-rays, significant numbers of photoelectron are generated by photoionization of the heavy atoms in the gas and grains. These electrons can excite, ionize, and dissociate molecular hydrogen (Shull & Beckwith 1982).

High-resolution spectra of the $np\sigma\ ^1\Sigma_u^+$ and $np\pi\ ^1\Pi_u$ Rydberg series of molecular hydrogen have been studied primarily by photoabsorption, photonionzation, and nonlinear laser techniques. Combination of a low-temperature high-resolution photoabsorption studies in the 765–835 Å region (Herzberg & Jungen 1972) and low-temperature photoionization studies in the 745–805 Å region (Demher & Chupka 1976) with multichannel quantum defect analysis have yielded a good description of channel interactions (Jungen & Atabek 1977; Herzberg & Jungen 1972), predissociation (Jungen 1984), and rovibrational autoionization (Raoult & Jungen 1981; Cornaggia, Giusti-Suzor, & Jungen 1987; Pratt et al. 1990, 1992; Dehmer et al. 1992) for the high-lying Rydberg states. Photodissociation studies by

[1] National Research Council Research Associate.
[2] Present address: Laboratorie Traitement du Signal et Instrumentation, CNRS 5516, 23 rue Dr. P. Michelon, 42023 Saint-Etiene Cedex 2, France.

Guyon, Breton, & Glass-Maujen (1979), Glab & Hessler (1987, 1990), Beswick & Glass-Maujean (1987), Glass-Maujean, Frohlich, & Beswick (1988), and McCormack et al. (1993) have contributed significantly to our understanding of the predissociation of the $np\sigma\ ^1\Sigma_u^+$ and $np\pi\ ^1\Pi_u$ Rydberg series. Spectroscopic works on H_2 prior to 1979 have been summarized by Huber & Herzberg (1979). Laboratory studies between 1979 and 1994 have been reviewed by Roncin & Launay (1994), who have also provided extensive tabulation of emission lines observed in their discharge studies. More recently, chemical reactions of H_2 $np\sigma$ and $np\pi$ Rydberg series with excited H atoms or H_2 molecules have been investigated by Pratt et al. (1994) and Dehmer & Chupka (1995). Ubachs and coworkers have also performed several experimental studies of H_2 and its isotope analogs in the EUV region at sub-Doppler resolution using nonlinear laser techniques (Hinnen et al. 1994a, 1994b, 1995; Reinhold, Hogervorst, & Ubachs 1996, 1997; Hogervorst et al. 1998). They also discussed the possibility of H_2 in excited Rydberg states as the carrier of the diffuse interstellar bands (Hinnen & Ubachs 1995, 1996; Ubachs, Hinnen, & Reinhold 1997). However, no high-resolution studies of electron-impact induced emission of H_2 in the EUV region have yet been reported.

The $np\sigma\ ^1\Sigma_u^+$ and $np\pi\ ^1\Pi_u$ Rydberg series have also been studied theoretically. Jungen & Atabek (1977) calculated the nonadiabatic energies of the two Rydberg series with multichannel quantum defect theory. Wolniewicz & Dressler (1988, 1992) and Senn, Quadrelli, & Dressler (1988) have calculated the nonadiabatic couplings among the $B\ ^1\Sigma_u^+$, $C\ ^1\Pi_u$, $B'\ ^1\Sigma_u^+$, and $D\ ^1\Pi_u$ states. Some of the results have been utilized to calculate the $B\ ^1\Sigma_u^+–X\ ^1\Sigma_g^+$, $C\ ^1\Pi_u–X\ ^1\Sigma_g^+$, $B'\ ^1\Sigma_u^+–X\ ^1\Sigma_g^+$, and $D\ ^1\Pi_u–X\ ^1\Sigma_g^+$ transition probabilities by Abgrall et al. (1987, 1993a, 1993b, 1994, 1997) and Abgrall & Roueff (1989).

We have previously reported a high-resolution ($\Delta\lambda = 0.136$ Å) study of electron-impact–induced emission spectra of H_2 in the FUV region (1140–1700 Å) under optically thin conditions (Liu et al. 1995). We showed that models utilizing Allison & Dalgarno (1970) band transition probabilities partitioned by Hönl-London factors yield incorrect intensities when local perturbations and the rotational dependence of the transition dipole matrix element are not negligible. We have also shown that both discrete and continuum $B\ ^1\Sigma_u^+–X\ ^1\Sigma_g^+$ and $C\ ^1\Pi_u–X\ ^1\Sigma_g^+$ transition probabilities calculated by Abgrall et al. (1987, 1993a, 1993b, 1993c) and Abgrall & Roueff (1989) accurately reproduce the relative experimental intensities and correctly account for the effects of $B\ ^1\Sigma_u^+–C\ ^1\Pi_u^+$ couplings and large centrifugal distortion potentials (Liu et al. 1995; Abgrall et al. 1997). However, as a part of our FUV study, we noted that the $B'\ ^1\Sigma_u^+$ and $D\ ^1\Pi_u$ emission cross sections obtained by Ajello et al. (1984, 1988) from their low-resolution (~ 5 Å) study overestimated the emission intensities of some vibrational bands of the $B'\ ^1\Sigma_u^+–X\ ^1\Sigma_g^+$ and $D\ ^1\Pi_u–X\ ^1\Sigma_g^+$ transitions by 200%–400%. Since the predissociation yields reported by Ajello et al. are closely related to the emission cross section, the FUV work strongly suggested large errors in the reported predissociation yields and excitation cross sections.

As a continuation of our experimental program, we report the first high-resolution electron-impact study of molecular hydrogen emission in the EUV region (900–1200 Å). Specifically, the high-resolution spectrum enables us to obtain well-resolved rotational lines of different band systems and to examine the relative accuracy of the calculated $B\ ^1\Sigma_u^+–X\ ^1\Sigma_g^+$, $C\ ^1\Pi_u–X\ ^1\Sigma_g^+$, $B'\ ^1\Sigma_u^+–X\ ^1\Sigma_g^+$ and $D\ ^1\Pi_u–X\ ^1\Sigma_g^+$ transition probabilities of Abgrall et al. (1987, 1989, 1993a, 1993b, 1993c, 1994) in certain spectral regions. We then utilize the calculated $B\ ^1\Sigma_u^+–X\ ^1\Sigma_g^+$, $C\ ^1\Pi_u–X\ ^1\Sigma_g^+$, and $D\ ^1\Pi_u^-–X\ ^1\Sigma_g^+$ transition probabilities and recently determined excitation functions (Liu et al. 1998) to obtain calibrated relative intensities. Emission cross sections of the $B'\ ^1\Sigma_u^+$, $B''\ ^1\Sigma_u^+$, $D\ ^1\Pi_u$, $D'\ ^1\Pi_u$, and $D''\ ^1\Pi_u$ states are measured from their individual line emission intensities relative to those of $B\ ^1\Sigma_u^+–X\ ^1\Sigma_g^+$, $C\ ^1\Pi_u–X\ ^1\Sigma_g^+$, and $D\ ^1\Pi_u^-–X\ ^1\Sigma_g^+$ transitions. Nonradiative yields are inferred by comparing the emission cross section with estimated excitation cross sections.

The organization of the present paper is as follows. Section 2 gives a brief description of the experimental apparatus used to measure the EUV spectrum. Experimental difficulties such as compromises between signal-to-noise ratio, data acquisition time, and optical thickness are discussed. Methods employed to estimate the effective column densities in the crossed-beam configuration are also described. Section 3 provides a concise description of electron-impact–induced emission intensities and the theoretical model used to analyze the observed spectral intensities. Section 4 deals with the analysis of spectra. A comparison of the relative intensities between observed and synthetic spectra over a number of narrow wavelength regions permits an examination of the relative accuracy of the calculated transition probabilities in these spectral regions. The instrumental sensitivity curve is derived by comparing the (raw) observed and synthetic spectra. The sensitivity curve is used, in turn, to calibrate the (raw) emission spectra obtained at 100 eV. Emission intensities from the $B'\ ^1\Sigma_u^+$, $B''\ ^1\Sigma_u^+$, $D'\ ^1\Pi_u$, and $D''\ ^1\Pi_u$ states are obtained from the calibrated spectra and are summed. The emission cross sections for these states are established by their relative intensities to $B\ ^1\Sigma_u^+–X\ ^1\Sigma_g^+$, $C\ ^1\Pi_u–X\ ^1\Sigma_g^+$, and $D\ ^1\Pi_u^-–X\ ^1\Sigma_g^+$ transitions that are free from predissociation and autoionization and whose emission cross sections are known (Liu et al. 1998) or can be calculated reliably from theoretical oscillator strength (Abgrall et al. 1994). In § 5, the emission yields are obtained by comparing the derived emission cross sections with estimated excitation cross sections. The implications of these emission yields are also discussed. Finally, § 6 summarizes the results of the present work.

2. EXPERIMENTAL SETUP

The essential features of the experimental setup have been described in detail by Liu et al. (1995). So, we will briefly outline common features of the setup and stress the differences between the present and the previous experimental configurations. Our experimental system consists of a 3 m VUV spectrometer (Acton VM-523-SG) and an electron collision chamber. Electrons produced by heating a thoriated tungsten filament are collimated with an axially symmetric magnetic field of ~ 100 G and accelerated to a kinetic energy of 100 eV. The accelerated electrons, which move horizontally, collide with a vertical beam of molecular hydrogen gas formed by a capillary array. The cylindrical interaction region is about ~ 3 mm in length and ~ 2 mm in diameter. Optical emission from electron-impact–excited H_2 is dispersed by the spectrometer, which has an aperture

ratio of f/28.8 and a field of view of 3.8 mm (horizontal) by 2.4 mm (vertical). The dispersed radiation is detected with a channel electron multiplier (Galileo 4503) coated with CsI. A Faraday cup is used to minimize backscattered electrons and monitor the electron beam current.

Unlike the emissions in the FUV region, a number of transitions in the EUV region involve the $v_i = 0$ (resonance) level of the $X\ ^1\Sigma_g^+$ state. If the density of H_2 is too high, the resonance self-absorption can be significant. In particular, self-absorption is problematic for the strong emissions from the $v_j = 0$–4 levels of the $C\ ^1\Pi_u$ state to the $v_i = 0$ level of the ground $X\ ^1\Sigma_g^+$ state. In order to measure the relative intensities accurately, the resonance self-absorption has to be minimized by reducing the number density of molecular hydrogen. On the other hand, this reduction in the density of H_2 results in weaker primary emission intensities, which is in conflict with the desired spectral high resolution and good signal-to-noise ratio, especially for the $B''\ ^1\Sigma_u^+$–$X\ ^1\Sigma_g^+$, $D'\ ^1\Pi_u$–$X\ ^1\Sigma_g^+$, and $D''\ ^1\Pi_u$–$X\ ^1\Sigma_g^+$ transitions, whose intensities are very weak. Thus, compromises between sample pressure, spectral resolution, signal-to- noise ratio, and data acquisition time have to be made.

To increase the sensitivity in the EUV region, the present experiment utilizes a custom-coated B_4C concave grating with 1200 grooves mm^{-1}. The grating, 104 × 65 mm in size, is blazed at 1200 Å with an angle of 4°7′. It has an efficiency in first order of 38.2%, 38.6%, and 37.6% at 920, 1025, and 1215 Å, respectively. The custom coating of B_4C was performed at NASA Goddard Space Flight Center. The thickness of the coating is 508 Å. In comparison with the previously used $Al + MgF_2$ coating, the B_4C coating increases the sensitivity by a factor of 1.6–4 in the 800–1150 Å region.

Since the EUV spectral region is more congested than the FUV spectral region, it was decided that the spectral resolution should not be lower than 0.125 Å FWHM. Emission spectra in the 800–1440 Å region were acquired in first order with a slit width of 40 μm. The spectral resolution of the experiment was about 0.115 Å as measured at zero order. However, the wavelength increment was increased to 0.040 Å per step, which yielded a FWHM of about three steps. Owing to the general weakness of the $B''\ ^1\Sigma_u^+$–$X\ ^1\Sigma_g^+$, $D'\ ^1\Pi_u$–$X\ ^1\Sigma_g^+$, and $D''\ ^1\Pi_u$–$X\ ^1\Sigma_g^+$ transitions, each data point was integrated for about 70 s, which resulted in a total acquisition time of ~13 days. To reduce the degree of resonance absorption, the H_2 pressure was lowered from 3×10^{-4} torr (which was used for the previous FUV study by Liu et al. 1995) to 1.2×10^{-5} torr. Because pressure was measured on the H_2 flow at about 10 cm downstream of the collision region, the reading really represents the steady state background pressure in the chamber. Owing to the large pressure gradient in the crossed-beam measurement, the background pressure reading is not a reliable indicator of the H_2 number density in the collision region (see below). However, it was used as a convenient relative indicator of the number density and as a measurement of any pressure fluctuations (<2%) during the scan.

The wavelength scale of the observed spectrum was established by assuming a uniform grating step size and by using the absolute wavelength of the H Lyman series emissions. The mechanical limitation of the stepping motor, and, more importantly, the slight temperature fluctuation of the spectrometer (±0°.3 C) during the scan resulted in significant slowly varying nonuniform wavelength shifts. The wavelength error could be estimated by comparing the present observed spectra of H_2 with the model spectra of H_2, which utilizes the experimentally derived energy levels of Roncin & Launay (1994). The largest wavelength error, as measured from the extremes of negative and positive shifts, was found to be 0.09 Å. As frequencies of many strong transitions of H_2 have been accurately measured in the previous studies, the effect of the small wavelength deviation can be reduced by aligning the observed and model spectra in 10 Å intervals over strong features. Hence, the wavelength shifts did not cause any significant problems for the analysis reported in the present paper.

The crossed-beam measurement introduces a large pressure gradient in the collision region. To account accurately for any resonance self-absorption, the effective column density of the experiment must be known. Two methods were used to estimate the effective column density. The first method involved a comparison between the spectral intensities measured in the swarm and crossed-beam configuration. First, the spectral intensity of a strong nonresonance transition such as the $Q(1)$ line of the (0, 2) Werner band was recorded at the operating sample pressure (i.e., chamber background pressure reading 1.2×10^{-5} torr) in the crossed-beam mode. Then, without changing any other experimental conditions, the measurement was repeated in the swarm mode. The collision chamber was slowly filled with H_2 gas until the same gauge pressure was reached. After the system had stabilized, the intensity of the same nonresonance spectral feature was measured. At an operating background pressure reading of 1.2×10^{-5} torr, the spectral intensity measured in the swarm mode was found to be 6.5 ± 0.4 times weaker than the corresponding intensity in the crossed-beam mode. Since there is no pressure gradient in the swarm measurement, its H_2 foreground column density is simply the product of a uniform number density and optical path length, which is 11.05 cm. The effective foreground column density for the crossed-beam mode is 6.5 ± 0.4 times the foreground column density of the swarm mode and is determined to be $(2.7 \pm 0.2) \times 10^{13}$ cm^{-2}. This number, however, likely represents the upper limit for actual foreground column density in the crossed-beam mode because of the finite viewing angle of the detection system. The electron-H_2 interaction region was larger in the swarm measurement than in the crossed-beam measurement. With the arrangement of the collision chamber and detection system optimized for the crossed-beam mode, certain portions of spectral emission may not be detected efficiently or may not even be detected in the swarm measurement. While the effect of the finite field view is somewhat difficult to quantify, we estimate that it inflates the foreground column density of the crossed-beam mode by 10%–15%. After the effect of the finite view region of the detection system is taken into account, the effective column density of the crossed-beam experiment is obtained as $(2.3 \pm 0.6) \times 10^{13}$ cm^{-2}.

The second method of estimating effective foreground column density involves a comparison of synthetic spectra with relative intensities of strong resonance transitions obtained at different foreground column densities. The model considers resonance fluorescence excitation with a standard absorption and curve-of-growth subroutine (see eqs. [2a]–[2c] in § 3). In the present experiment, fluorescence excitation is so small when compared with the primary electron-impact excitation that any subsequent

emission due to fluorescence excitation can be safely neglected (see § 4.1.1). The net effect of the resonance excitation is the attenuation of the primary emission that ends at the $v_i = 0$ level of the $X\ ^1\Sigma_g^+$ state. Since the attenuation has a nonlinear dependence on its quantum state column density, comparison of the synthetic spectra against the observed resonance spectra enables an estimation of the foreground column density. The relative intensities of the $R(0)$, $R(1)$, $R(2)$, $Q(1)$, and $P(3)$ lines for each of the ($v_C = 0$–5, $v_X = 0$) Werner bands, which have large oscillator strengths and cover fairly wide quantum state column density ranges, are selected for the comparison. The selected lines for each of the Werner bands all lie within 6 Å spectral regions. Since the instrumental sensitivity variation is less than 1% in each of these 6 Å regions, comparison can be performed with the raw (uncalibrated) spectra. The effective column density estimated by this method is $(2.0 \pm 0.3) \times 10^{13}$ cm^{-2}, which is consistent with the value $(2.3 \pm 0.6) \times 10^{13}$ cm^{-2} obtained from the swarm and crossed-beam comparative measurements.

3. THEORY

The volumetric photon emission rate (I) from electron-impact excitation is proportional to the excitation rate and emission branching ratio:

$$I(v_j, v_i; J_j, J_i) = g(v_j; J_j)\,\frac{A(v_j, v_i; J_j, J_i)}{A(v_j; J_j)} \times [1 - \eta(v_j, J_j)][1 - \kappa(\epsilon_{ij}, \zeta_i)]\ , \quad (1)$$

where the indices j and i refer to the upper and lower electronic state vibrational and rotational levels, respectively, and summation over the missing index is assumed. v and J refer to vibrational and rotational quantum numbers. $A(v_j, v_i; J_j, J_i)$ is the Einstein spontaneous transition probability for emission from level (v_j, J_j) to level (v_i, J_i), and $A(v_j, J_j)$ is the total radiative transition probability for level (v_j, J_j). $\eta(v_j, J_j)$ represents the yield of nonradiative processes. Under the present experimental conditions, collision deactivation is 10^4–10^5 times slower than radiative decay and is therefore negligible. So, $\eta(v_j, J_j)$ normally includes predissociation, dissociation, and autoionization. As discussed in § 4.1.3, the nonradiative yield, η, is zero for all the $B\ ^1\Sigma_u^+$–$X\ ^1\Sigma_g^+$, $C\ ^1\Pi_u$–$X\ ^1\Sigma_g^+$ and $D\ ^1\Pi_u^-$–$X\ ^1\Sigma_g^+$ bands and the transitions involving the $D\ ^1\Pi_u^+$ levels that lie below the H(1s)+H(2ℓ) dissociation limit. $\kappa(\epsilon_{ij},\zeta_i)$ in equation (1) an is attenuation factor that measures the self-absorption for the resonance transitions. κ_{ij} relates the extinction coefficient, ϵ_{ij}, and the quantum state column density, ζ_i, by

$$\kappa_{ij} = 1 - \frac{1}{1.0 + 0.9948(\epsilon_{ij}\zeta_i)^{1.44}}\ , \quad (2a)$$

$$\epsilon_{ij} = \frac{2.472 \times 10^{-6}}{\nu^3 T^{0.5}}\,\frac{2J_j + 1}{2J_i + 1}\,A(v_j, v_i; J_j, J_i)\ , \quad (2b)$$

$$\zeta_i = \frac{N(v_i, J_i)}{N(0, 0)Q_P}\,(N_t\ell)\ , \quad (2c)$$

where ν is the transition frequency in cm^{-1}, $N(v_i, J_i)$ is the population at the level i, Q_P is the partition function, and $N_t\ell$ is H_2 foreground column density in cm^{-2}. At $T = 300$ K, the fractional population, N_i/N_t, for $v_i \geq 1$ is less than 1.4×10^{-8}. Thus, the attenuation factor κ_{ij} due to resonance absorption vanishes unless v_i is 0.

The excitation rate, $g(v_j, J_j)$ of equation (1), represents the sum of the excitation rates from the rotational and vibrational levels of the $X\ ^1\Sigma_g^+$ state. It is proportional to the population of the molecule in the initial level, $N(v_i, J_i)$, the excitation cross section (σ_{ij}), and the electron flux (F_e):

$$g(v_j; J_j) = F_e \sum_i N(v_i, J_i)\sigma(v_i, v_j; J_i, J_j)\ , \quad (3)$$

where the cross section σ_{ij} is calculated from the analytical function (Shemansky, Ajello, & Hall 1985a; Shemansky et al. 1985b)

$$\frac{\sigma_{ij}}{\pi a_0^2} = 4 f_{ij}\,\frac{\mathrm{Ry}}{E_{ij}}\,\frac{\mathrm{Ry}}{E}\left[\frac{C_0}{C_7}\left(\frac{1}{X^2} - \frac{1}{X^3}\right) + \sum_{k=1}^{4}\frac{C_k}{C_7}\,(X - 1)^k \times \exp\,(-kC_8\,X)\right]\left[+\frac{C_5}{C_7} + \frac{C_6}{C_7}\,\frac{1}{X} + \ln(X)\right], \quad (4)$$

where a_0 and Ry are the Bohr radius and Rydberg constant, respectively; f_{ij} is the optical absorption oscillator strength; E and E_{ij} are the electron impact and transition energies, respectively; and $X = E/E_{ij}$. The coefficients C_k/C_7 ($k = 0$–6) and C_8 are determined by fitting the experimentally measured relative excitation function. For the present work, C_k/C_7 ($k = 0$–6) and C_8 determined by Liu et al. (1998) for the Lyman and Werner band systems of H_2 are used for the direct excitation of the $B\ ^1\Sigma_u^+$–$X\ ^1\Sigma_g^+$, $C\ ^1\Pi_u$–$X\ ^1\Sigma_g^+$, $B'\ ^1\Sigma_u^+$–$X\ ^1\Sigma_g^+$, and $D\ ^1\Pi_u$–$X\ ^1\Sigma_g^+$ band systems. In addition to the direct excitation, cascade excitation from the excited $^1\Sigma_g^+$ states such as the $EF\ ^1\Sigma_g^+$ state is also significant (Ajello et al. 1984; Liu et al. 1995; Abgrall et al. 1999). While the $EF\ ^1\Sigma_g^+$–$C\ ^1\Pi_u$ cascade excitation is generally believed to be negligible, the $EF\ ^1\Sigma_g^+$–$B\ ^1\Sigma_u^+$ transition is known to significantly enhance the emission from the low v_j levels of the $B\ ^1\Sigma_u^+$ state. The cascade excitation model recently detailed by Abgrall et al. (1999) is used for the present analysis. Figure 1 shows the synthetic spectra for the $B\ ^1\Sigma_u^+$–$X\ ^1\Sigma_g^+$, $C\ ^1\Pi_u$–$X\ ^1\Sigma_g^+$, $B'\ ^1\Sigma_u^+$–$X\ ^1\Sigma_g^+$, and $D\ ^1\Pi_u$–$X\ ^1\Sigma_g^+$ band systems when self-absorption is negligible.

Owing to the possibilities of $^1\Sigma_u^+$–$^1\Pi_u^+$ perturbations and the rotational dependence of the transition dipole matrix elements, the present work defines the total excitation cross section of an electronic band system as the statistically averaged total excitation cross section,

$$\sigma_s = \frac{1}{N_0\,Q_P}\sum_{i,j}\sigma_{ij}N_i\ . \quad (5)$$

4. ANALYSIS AND RESULTS

4.1. *Relative Accuracy of the Model*

4.1.1. *Self-Absorption*

For analysis of the present work, we adopt a foreground column density of 2.0×10^{13} cm^{-2}. Under this condition, the self-absorption model utilizing equations (2a)–(2c) shows that the largest attenuations for the $B'\ ^1\Sigma_u^+$ and $D\ ^1\Pi_u$ states are 1.8% and 2.7%, which occur at the 1(2, 0)R line of $B'\ ^1\Sigma_u^+$–$X\ ^1\Sigma_g^+$ and the 1(1, 0)Q line of $D\ ^1\Pi_u$–$X\ ^1\Sigma_g^+$, respectively. Thus, all the transitions of the $B'\ ^1\Sigma_u^+$–X

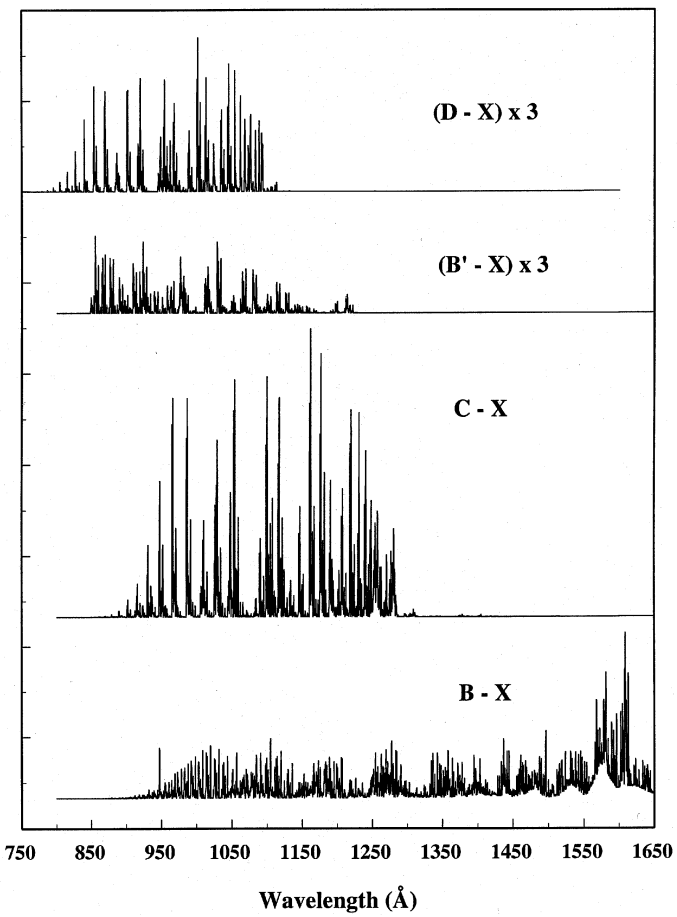

FIG. 1.—Calculated electron-impact–induced emission spectra of the $B\ ^1\Sigma_u^+–X\ ^1\Sigma_g^+$, $C\ ^1\Pi_u–X\ ^1\Sigma_g^+$, $B'\ ^1\Sigma_u^+–X\ ^1\Sigma_g^+$, and $D\ ^1\Pi_u–X\ ^1\Sigma_g^+$ band systems for H_2 molecule at 300 K and 100 eV. The intensities of the $B'\ ^1\Sigma_u^+–X\ ^1\Sigma_g^+$ and $D\ ^1\Pi_u–X\ ^1\Sigma_g^+$ band systems have been expanded by a factor of 3. Note that the strong line at 946.98 Å in the Lyman band system corresponds to the $R(1)$ line of the (14, 0) band, whose intensity increases by a factor of ~ 7 as a result of coupling between the $v_j = 3$ of the $C\ ^1\Pi_u^+$ state and $v_j = 14$ of the $B\ ^1\Sigma_u^+$ state (see text and Liu et al. 1995).

$^1\Sigma_g^+$ and $D\ ^1\Pi_u–X\ ^1\Sigma_g^+$ band systems can be considered as optically thin. Since the oscillator strengths for the $B''\ ^1\Sigma_u^+–X\ ^1\Sigma_g^+$, $D'\ ^1\Pi_u–X\ ^1\Sigma_g^+$, and $D''\ ^1\Pi_u–X\ ^1\Sigma_g^+$ systems are even smaller, the effect of self-absorption does not need to be considered for these band systems.

For certain vibrational bands of the $B\ ^1\Sigma_u^+–X\ ^1\Sigma_g^+$ and $C\ ^1\Pi_u–X\ ^1\Sigma_g^+$ systems, however, resonance absorption is very significant. In general, for a given (v_j, $v_i = 0$) band, the strongest attenuation occurs at the $Q(1)$ transition for the $C\ ^1\Pi_u^-$ state and at $R(1)$ lines for the $B\ ^1\Sigma_u^+$ and $C\ ^1\Pi_u^+$ states. In the Lyman system, several of the largest self-absorptions are 11%, 12%, 13%, 11%, 10%, and 10.1% for the $R(1)$ emission of the (5, 0), (6, 0), (7, 0), (8, 0), (9, 0), and (14, 0) bands, respectively. For the Werner system, resonance absorption attenuates the $Q(1)$ emission of the ($v_C = 0$–5, 0) bands by factors 15%, 24%, 23%, 17%, 11%, and 6%, respectively, and the corresponding $R(1)$ lines by 13%, 22%, 23%, 6%, 8%, and 5%, respectively.

While resonance fluorescence excitation attenuates certain transitions of the Lyman and Werner bands significantly, its effect on overall emission intensities is insignificant. For example, at the adopted foreground column density, the attenuation for the total Lyman and Werner band emission intensities between 900 and 1150 Å is only 1.4% and 3.4%, respectively.

It should be pointed out that the above calculations implicitly assume the precision of the self-absorption model and adopted foreground column density. Nevertheless, the two independent measurements of foreground column density described in § 2 yielded values that agree with each other, supporting the self-absorption model and adopted foreground column density. The fact that the self-absorption model can reproduce the relative intensities of the resonance rotational lines in each of the ($v_C = 0$–5, $v_X = 0$) (see § 4.3) bands provides further confidence in the self-absorption model.

If the foreground column density is raised from 2.0×10^{13} cm^{-2} to 2.5×10^{13} cm^{-2}, the most significant intensity attenuation, at the $Q(1)$ line of the (1, 0) band for the Werner system, increases from 24% to 30%. In the very unlikely scenario that the self-absorption model carries a 20% error, it introduces only 6% of error in the worst case. Since resonance excitation attenuates the overall Werner band emission between 900 and 1150 Å by only 3.4%, any errors in the self-absorption model and foreground column density are, in general, negligible.

4.1.2. *Relative Accuracy of Cross Sections and Transition Probabilities*

In the limit of no nonradiative processes and no resonance absorptions, the accuracy of the model depends on the precision of the excitation function coefficients (C_k/C_7 and C_8), calculated transition probabilities and oscillator strength of equations (1) and (4). Since the present work measures the relative spectral intensities, only the relative accuracy of the cross section and transition probabilities needs to be discussed.

The absolute error for the Lyman and Werner band cross sections at 100 eV, as reported by Liu et al. (1998), is less than 15%. The relative cross section error between the $B^1\Sigma_u^+$ and $C\ ^1\Pi_u$ states at the same energy, however, is significantly lower and is estimated to be less than 2% (see Table 2 of Liu et al. 1998). Thus, from a relative intensity point of view, the error in excitation function coefficients can be safely neglected for the $B\ ^1\Sigma_u^+–X\ ^1\Sigma_g^+$ and $C\ ^1\Pi_u–X\ ^1\Sigma_g^+$ transitions. The excitation coefficients for the $B'\ ^1\Sigma_u^+$ and $D\ ^1\Pi_u$ states have not been measured. However, since $B'\ ^1\Sigma_u^+$ and $B\ ^1\Sigma_u^+$, and $D\ ^1\Pi_u$ and $C\ ^1\Pi_u$ belong to the same Rydberg series and since the excitation shape functions of the $B\ ^1\Sigma_u^+$ and $C\ ^1\Pi_u$ states are found to be the same within experimental error (Liu et al. 1998), it seems reasonable to assume that the excitation function coefficients of the $B'\ ^1\Sigma_u^+$ and $D\ ^1\Pi_u$ states are also the same as those of the $B\ ^1\Sigma_u^+$ and $C\ ^1\Pi_u$ states. Moreover, relative cross section errors due to the difference in excitation shape functions at 100 eV (which roughly corresponds to $X = 7$–8 for $B'\ ^1\Sigma_u^+$ and $D\ ^1\Pi_u$ states) are expected to be a few percent. Finally, because the band oscillator strength of the $B'\ ^1\Sigma_u^+–X\ ^1\Sigma_g^+$ and $D\ ^1\Pi_u–X\ ^1\Sigma_g^+$ systems are significantly smaller than those of the Lyman and Werner bands, the errors due to the assumption on the relative emission intensities are unlikely to be significant.

The relative accuracy of the model spectra is thus primarily determined by the relative precision of the transition probabilities (and oscillator strengths), which, in turn, depend on the accuracy of the electric dipole matrix elements and the transition frequencies. The transition prob-

abilities calculated by Abgrall et al. (1993a, 1993b, 1993c, 1994) are obtained by solving a system of four coupled Schrödinger equations for the $B\ ^1\Sigma_u^+$, $C\ ^1\Pi_u$, $B'\ ^1\Sigma_u^+$, and $D\ ^1\Pi_u$ states based on the ab initio transition moments and potentials calculated by Dressler & Wolniewicz (1985, 1986), Ford et al. (1975), Rothenberg & Davidson (1967), and Wolniewicz & Dressler (1988, 1992). To improve the accuracy, Abgrall et al. have adjusted the ab initio potentials so that the calculated transition frequencies for the lowest J levels agree with experimental values. As a result, all calculated transition frequencies deviate by less than 1.5 cm^{-1} from the high-resolution experimental frequencies of Roncin & Launay (1994). As the observed transition frequencies are of the order $\sim 1 \times 10^5$ cm^{-1}, uncertainties in transition frequencies are completely negligible, and uncertainties in transition probabilities arise almost exclusively from the transition moments.

The $B\ ^1\Sigma_u^+$–$X\ ^1\Sigma_g^+$ and $C\ ^1\Pi_u$–$X\ ^1\Sigma_g^+$ transition moments calculated by Dressler & Wolniewicz (1985) differ less than 0.2% from those calculated by Wolniewicz (1969) when the internuclear distance is smaller than 2.1 Å. The differences become larger at longer internuclear distance with the largest difference, 2.3%, occurring at 3.7 Å. Moreover, a more recent calculation by Wolniewicz (1995) obtained a $C\ ^1\Pi_u$–$X\ ^1\Sigma_g^+$ transition moment, which differs by less than 0.06% from that of Dressler & Wolniewicz (1985). As the error in the recent Wolniewicz's calculation is estimated to be smaller than 0.01%, it appears that the relative error in transition probabilities due to the uncertainty in the ab initio transition moments is at most 5%. Furthermore, the probable Lyman and Werner transitions are observed in the region in which the internuclear distance is much shorter than 3.7 Å. The relative transition probability error due to the uncertainty of the transition moment is generally much smaller than 4.7%. Further evidence on the relative accuracy of the transition probabilities comes from our previous study (Liu et al. 1995), where it was shown that the discrete transition probabilities calculated by Abgrall et al. (1993a, 1993b) accurately describe both perturbation and the J-dependence of the transition dipole matrix elements. Hence it can be confidently concluded that the relative error in Lyman and Werner transition probabilities for strong or moderately strong transitions is less than 3%. While the relative error for weak transitions can be significantly larger, their contributions to the observed emission intensities are negligible.

The $B'\ ^1\Sigma_u^+$–$X\ ^1\Sigma_g^+$ and $D\ ^1\Pi_u$–$X\ ^1\Sigma_g^+$ transition moments used to obtain the transition probabilities are calculated by Ford et al. (1975) and Rothenberg & Davidson (1967). Since these transition moments have not been calculated as extensively as their Lyman and Werner counterparts, it is difficult to assess their accuracies with respect to the Lyman and Werner bands. However, the lifetimes of $J_j = 1$ of the $v_j = 3$–15 levels of the $D\ ^1\Pi_u^-$ state measured by Glass-Maujean et al. (1985b) are in fairly good agreement with those calculated by Glass-Maujean (1984), who considered the band transition probabilities for the $D\ ^1\Pi_u$–$X\ ^1\Sigma_g^+$ transition only for the calculation of lifetimes. In addition, the lifetime measurement has confirmed the prediction of Rothenberg & Davidson that the variation of the dipole moment with internuclear distance is small. Finally, a more extensive calculation by Abgrall, Roueff, & Drira (2000) utilizing the recent $D\ ^1\Pi_u$–$X\ ^1\Sigma_g^+$ transition moment obtained by Drira (1999) has produced a set of $D\ ^1\Pi_u$–$X\ ^1\Sigma_g^+$ transition probabilities that differs by less than $\sim 10\%$ from that reported by Abgrall et al. (1994). It should be noted that while the error in the $D\ ^1\Pi_u$–$X\ ^1\Sigma_g^+$ and $B'\ ^1\Sigma_u^+$–$X\ ^1\Sigma_g^+$ transition moments is probably larger than that in the $B\ ^1\Sigma_u^+$–$X\ ^1\Sigma_g^+$ and $C\ ^1\Pi_u$–$X\ ^1\Sigma_g^+$ transition moments, excitation cross sections of the $B'\ ^1\Sigma_u^+$ and $D\ ^1\Pi_u$ state are also significantly smaller than their $B\ ^1\Sigma_u^+$ and $C\ ^1\Pi_u$ counterparts. Furthermore, the strong predissociation at the $D\ ^1\Pi_u^+$ levels that are above the H(1s) + H(2ℓ) dissociation limit further reduces their emission intensities. Thus, the error propagated into the spectral intensities should probably be comparable to those of the Lyman and Werner bands unless the spectral region is dominated by the $B'\ ^1\Sigma_u^+$–$X\ ^1\Sigma_g^+$ and $D\ ^1\Pi_u$–$X\ ^1\Sigma_g^+$ transitions.

The relative accuracy of the transition probabilities discussed so far applies only when the rovibronic couplings among the Rydberg states are insignificant. When the coupling is not negligible, eigenfunctions of the interacting levels are mixed and the accuracy of the transition probabilities also depends on the accuracy of the mixing coefficients. The most important coupling for H_2 is the heterogeneous L-uncoupling that takes place between the $^1\Sigma_u^+$ and the $^1\Pi_u^+$ states. The homogeneous nonadiabatic coupling which occurs between $^1\Sigma_u^+$–$^1\Sigma_u^+$, $^1\Pi_u^+$–$^1\Pi_u^+$, and $^1\Pi_u^-$–$^1\Pi_u^-$ states is also possible. Given that the $B\ ^1\Sigma_u^+$ and $C\ ^1\Pi_u$ states are the two lowest member of the Rydberg series, the perturbation must be primarily from the $B'\ ^1\Sigma_u^+$ and $D\ ^1\Pi_u$ states or between the $B\ ^1\Sigma_u^+$ and $C\ ^1\Pi_u^+$ states. The perturbations involving the $B\ ^1\Sigma_u^+$ and $C\ ^1\Pi_u$ states are expected to be accurately considered in the four-state coupling calculation of Abgrall et al. (1993a, 1993b, 1993c, 1994). Indeed, our previous FUV measurement (Liu et al. 1995) has shown that calculations of Abgrall et al. accurately describe the strong perturbations between $J_j = 1$, 2, and 3 of the $v_B = 14$ and $v_{C+} = 3$ levels (see Figs. 4 and 5 and Table 2 of Liu et al. 1995) and between $J_j = 3$ and 4 of the $v_B = 12$ and $v_{C+} = 2$ levels. For the $B'\ ^1\Sigma_u^+$ and $D\ ^1\Pi_u$ states, the situation is different because they can be perturbed by the lower $B\ ^1\Sigma_u^+$ and $C\ ^1\Pi_u$ states and higher $np\sigma$ and $np\pi$ ($n \geq 4$) states. While couplings with the $B\ ^1\Sigma_u^+$ and $C\ ^1\Pi_u$ have been considered in the calculations of Abgrall et al., couplings with higher ($n \geq 4$) $np\sigma$ and $np\pi$ states have been neglected. Any significant couplings of the $B'\ ^1\Sigma_u^+$ and $D\ ^1\Pi_u^+$ with the $B''\ ^1\Sigma_u^+$ and/or $D'\ ^1\Pi_u^+$ states, for instance, will certainly make the calculated transition probabilities less accurate. Namioka (1964) has shown the couplings of the $v = 1$–4 levels of the $B'\ ^1\Sigma_u^+$ state to the $v = 0$–2 levels of the $D\ ^1\Pi_u^+$ state, the $v = 5$ and 6 levels of the $B'\ ^1\Sigma_u^+$ state to the $v = 0$ level of the $D'\ ^1\Pi_u^+$, and the $v = 4$ level of the $B'\ ^1\Sigma_u^+$ state to the $v = 0$ level of the $B''\ ^1\Sigma_u^+$ state. Nevertheless, coupling of the $D\ ^1\Pi_u^-$ with higher $np\pi\ ^1\Pi_u^-$ is expected to be negligible because absorption studies have so far failed to reveal any significant perturbation for the $D\ ^1\Pi_u^-$ state (Namioka 1964; Takezawa 1970; Herzberg & Jungen 1972).

4.1.3. *Predissociation and Autoionization of the $np\sigma\ ^1\Sigma_u^+$ and $np\pi\ ^1\Pi_u$ Rydberg Series*

The dissociation energy and ionization energy of the $v_i = 0$ and $J_i = 0$ level of the $X\ ^1\Sigma_g^+$ state of H_2 are 36,118.11 cm^{-1}, and 124,417.507 cm^{-1}, respectively (Balakrishnam, Smith, & Stoicheff 1992, 1994). The dissociation energy for formation of H(1s) and H(2ℓ) is 118,377.06 cm^{-1}. For the levels that lie below the ionization potential, spontaneous

emission and predissociation compete to depopulate the excited states since collisional deactivation in the present experiment can be neglected completely. For the states that lie above 124417.507 cm^{-1} (Gilligan & Eyler 1992), autoionization can also compete to depopulate the excited states. In order to model the emission spectra accurately, the predissociation and autoionization yield, $\eta(v_j, J_j)$ of equation (1), needs to be known.

As mentioned in § 1, many experimental and theoretical investigations have been performed on the predissociation of the $np\sigma\ ^1\Sigma_u^+$ and $np\pi\ ^1\Pi_u$ Rydberg series. In general, the couplings between these Rydberg states and continuum of the $B'\ ^1\Sigma_u^+$ state is the primarily pathway for predissociation. Depending on the spatial symmetry of the Rydberg state, the magnitude of predissociation can vary significantly. The qualitative general rules can be summarized as follows:

1. Predissociation in the $B\ ^1\Sigma_u^+$ and $C\ ^1\Pi_u$ states is negligibly small. In the adiabatic approximation, both $B\ ^1\Sigma_u^+$ and $C\ ^1\Pi_u$ states correlate with the H(1s) + H(2p) limit, while the $B'\ ^1\Sigma_u^+$ state correlates with the H(1s) + H(2s) dissociation limit (Mulliken 1966). Rotation-vibrational levels of the $B\ ^1\Sigma_u^+$ and $C\ ^1\Pi_u$ states generally lie below their counterparts of the $B'\ ^1\Sigma_u^+$ state. Furthermore, transitions involving levels as high as 118,258 cm^{-1} ($v = 35$, $J = 1$) of the $B\ ^1\Sigma_u^+$ state, 118,297.71 cm^{-1} ($v = 11$, $J = 10$) of the $C\ ^1\Pi_u^+$ state, and 118,376.68 cm^{-1} ($v = 13$, $J = 2$) of the $C\ ^1\Pi_u^-$ state have been observed in the work of Glass-Maujean et al. (1985a) and Roncin & Launay (1994). Finally, any minor predissociation near the dissociation limit, if it exists, will be negligible in the present experiment as the Frank-Condon overlap between these high-lying levels and the $v_j = 0$ level of the $X\ ^1\Sigma_g^+$ state is very small. For instance, the value of A_{ji}/v_{ji}^3 of the $Q(2)$ transition of the (13,0) Werner band and $[P(2) + R(0)]$ transitions of the (34, 0) Lyman band fall by a factor of $\sim$160 and $\sim$360, respectively, from their counterparts of the (1, 0) Werner band and (7, 0) Lyman band (Abgrall et al. 1993a, 1993b; Glass-Maujean et al. 1985a).

2. Predissociations of the $np\pi\ ^1\Pi_u^-$ ($n \geq 3$) states are also very small because their couplings with the $B'\ ^1\Sigma_u^+$ state are not allowed by symmetry. Guyon et al. (1979) has suggested that the $np\pi\ ^1\Pi_u^-$ ($n \geq 3$) states can only be weakly predissociated by a coupling with the continuum of the $C\ ^1\Pi_u^-$ state. Since the $np\pi\ ^1\Pi_u^-$ series correlate adiabatically with the H(1s) + H(np) dissociation limits, the $3p\pi\ D\ ^1\Pi_u^-$ state would be the most energetically favorable one (in the $np\pi\ ^1\Pi_u^-$ series) for such coupling. In particular, if the coupling is of any significance, one expects that the levels that are close to the continuum levels of the $C\ ^1\Pi_u^-$ state and have significant Frank-Condon overlap would be especially susceptible to the predissociation. However, discharge emission studies of Abgrall et al. (1994) and Roncin & Launay (1994) do not indicate any significant predissociation at these levels. Thus, it can be concluded that the $np\pi\ ^1\Pi_u^-$ states decay by radiative emission.

3. The $np\pi\ ^1\Pi_u^+$ states are predissociated by the continuum of the $B'\ ^1\Sigma_u^+$ state. Depending on the principal quantum number, the predissociation yield can change significantly. The $v_j \geq 3$ levels of the $3p\pi\ ^1\Pi_u^+$ (i.e., $D\ ^1\Pi_u^+$) state, being the closest to the $3p\sigma\ ^1\Sigma_u^+$ state, are strongly predissociated (Julienne 1971; Fiquet-Fayard & Gallais 1972). Indeed, the $v_j \geq 3$ levels are known to be totally predissociated (Monfils 1961), and extensive experimental work of Abgrall et al. (1994) and Roncin & Launay (1994) failed to observe any emission from $v_j \geq 3$ levels. Experimental work by Glass-Maujean, Breton, & Guyon (1979) has obtained the lifetimes for $J_j = 2$ of $v_j = 3$–11 levels of the $D\ ^1\Pi_u^+$ state that range from 3.7×10^{-13} to 5.9×10^{-13} s. In contrast, the calculated lifetimes are (2.8–3.3) $\times 10^{-9}$ s for the $v_j = 0$–2 levels of the $D\ ^1\Pi_u^+$ state and (2.3–2.8) $\times 10^{-9}$ s for all the observed levels of the $D\ ^1\Pi_u^-$ state. The predissociation yields for the higher ($n > 3$) states are weaker than that of $D\ ^1\Pi_u^+$ state and generally decrease as the n increases. This is because the predissociation is of second order or accidental nature, which arises from either $np\pi\ ^1\Pi_u^+$–$3p\pi\ ^1\Pi_u^+$ coupling followed by $3p\pi\ ^1\Pi_u^+$–$3p\sigma\ ^1\Sigma_u^+$ predissociation, or $np\pi\ ^1\Pi_u^+$–$np\sigma\ ^1\Sigma_u^+$ coupling followed by $np\sigma\ ^1\Sigma_u^+$–$3p\sigma\ ^1\Sigma_u^+$ predissociation (Glass-Maujean, Breton, & Guyon 1978; Glass-Maujean 1979; Dehmer & Chupka 1995). Indeed, Guyon et al. (1979) have found that the predissociation yields of the $4p\pi\ D'\ ^1\Pi_u^+$ state to drop from 0.82 ± 0.1 to 0.6 ± 0.1 as v_j increases from 2 to 7.

4. The predissociation of the $np\sigma\ ^1\Sigma_u^+$ series arises primarily from their interaction with the $3p\sigma\ ^1\Sigma_u^+$ state. As n increases, the energy difference between the $np\sigma\ ^1\Sigma_u^+$ and $3p\sigma\ ^1\Sigma_u^+$ states also expands. Thus, the predissociation yields for the higher n states tend to be lower. The trend does not necessarily hold for every rovibration level as accidental perturbations may enhance the predissociation rate significantly.

Autoionization is an additional nonradiative channel as the level energy increases above the ionization limit. Because the potential energy curve of the H_2^+ ion and H_2 Rydberg states ion core generally have nearly identical shape in the region of small displacement, the vibrational propensity rule suggests that autoionization tends to take place with minimum vibrational quantum number changes (Berry 1966; Bardsley 1967; Chupka 1987). Hence, autoionization is generally inefficient for the low-n Rydberg states, which must autoionize with large changes in vibrational quantum number Δv. For example, while the $v_j \geq 6$ levels of the $D\ ^1\Pi_u$ state lie above the ionization limit, their autoionization must take place via a $\Delta v \geq 6$ process. Indeed, the experimental study of Dehmer & Chupka (1976) has shown that autoionization of the $D\ ^1\Pi_u$ state is negligibly small.

Based on the points summarized above, we conclude that the predissociation and autoionization yield, $\eta(v_j, J_j)$, is zero for all the observed transitions for the $B\ ^1\Sigma_u^+$–$X\ ^1\Sigma_g^+$, $C\ ^1\Pi_u$–$X\ ^1\Sigma_g^+$ and $D\ ^1\Pi_u^-$–$X\ ^1\Sigma_g^+$ band systems in the present experiment. For the $D\ ^1\Pi_u^+$–$X\ ^1\Sigma_g^+$ transition, the autoionization is also negligible. Moreover, transitions from the $v_j \geq 3$ levels have their $\eta(v_j, J_j) = 1$ because these levels are known to be completely predissociated. However, transitions from the $J_j \leq 6$ of the $v_j = 0$, 1, and 2 levels have their $\eta(v_j, J_j) = 0$, as these levels lie below the H(1s)+H(2ℓ) dissociation limit. Similarly, the $\eta(v_j, J_j)$ of the discrete levels of the $B'\ ^1\Sigma_u^+$ are also zero. The highest discrete level of the $B'\ ^1\Sigma_u^+$ state from which emission is observed is $v_j = 7$ and $J_j = 4$ (118,323.49 cm^{-1}), while the highest calculated discrete level is $v_j = 9$ and $J_j = 1$ (118,376.6 cm^{-1}) (Abgrall et al. 1994). We have included transitions involving the discrete levels of $v_j = 8$ and 9 in the model calculation. Since the excitation from $v_j = 8$ and 9 contribute only 0.5% to the total discrete $B'\ ^1\Sigma_u^+$–$X\ ^1\Sigma_g^+$ excitation, the inclusion is not

significant. Excitation into the continuum levels of the $B'\ ^1\Sigma_u^+$ state results in total dissociation.

4.2. *Calibration*

Once the values of $\kappa(\epsilon_{ij}, \zeta_i)$, $\eta(v_j, J_j)$ and relative accuracies of the transition probabilities are established, it is possible to produce the synthetic spectra according to equations (1)–(4) (Fig. 1) and utilize them to calibrate the observed spectra. The observed spectra were corrected for dark counts and fluctuations in pressure and electron beam current that occurred during data acquisition. To ensure an accurate calibration, the synthetic data were also convoluted with a triangular instrument line shape function with FWHM of 0.115 Å.

Spectral intensity calibration can be performed by comparing the observed raw and model intensities. However, since the model spectra consist of emissions from only the $B\ ^1\Sigma_u^+$, $C\ ^1\Pi_u$, $B'\ ^1\Sigma_u^+$, and $D\ ^1\Pi_u$ states, the comparison must be performed only in the regions in which the spectral intensities are completely dominated by emissions from these four states. Emission from the other Rydberg states tend to be insignificant in the longer wavelength regions. In the wavelength region longer than 930–940 Å, emissions from the $B\ ^1\Sigma_u^+$, $C\ ^1\Pi_u$, $B'\ ^1\Sigma_u^+$, and $D\ ^1\Pi_u$ states, except in a few isolated small intervals, completely dominate. These isolated spots include atomic hydrogen $n\ ^2P_{3/2,1/2}-^2S_{1/2}$ transitions for $n = 2, 3, 4, 5$, and 6 from dissociative excitation of H_2 and some weak emissions from the $n > 3$ Rydberg states that extend into the long-wavelength regions. By a careful selection of wavelength intervals, it is possible either to exclude the $n \geq 4$ Rydberg emission intensities from the selected interval or to make them negligibly small in comparison with the emission intensity from the $B\ ^1\Sigma_u^+$, $C\ ^1\Pi_u$, $B'\ ^1\Sigma_u^+$, and $D\ ^1\Pi_u$ states enclosed in the interval. Thus, for the emission spectra on the red side of 930 Å, the calibration by wavelength interval used by Liu et al. (1995) for the FUV spectra can be utilized. In the region shorter than 900 Å, the spectral congestion makes it difficult to find a region a few Å wide, where the emission intensities from the higher Rydberg states are negligible. In this region, the calibration should be done with the relative intensities of strong and isolated rotational lines (e.g., Q-branch or strong lines of the Lyman and Werner bands). For calibration of the wavelength regions on the blue side of 900 Å, several precautions must be taken. First, it is very important to correct any wavelength shift so that the emission intensities of the same set of transitions for both raw spectra and synthetic spectra are measured in the identical wavelength intervals. The synthetic spectra should also be convoluted with identical wavelength increment as the observed spectra. Moreover, the phase of the sampling in both sets of spectra should be matched. Finally, as the intensity comparison is made between the isolated lines, it is preferable that the transitions selected are not perturbed. The minor but significant wavelength shifts in the experimental spectra make the phase matching rather time-consuming. These precautions are generally not necessary for the calibration in the long wavelength where the integrated intensities over 10–20 Å wavelength intervals are compared.

The final calibration was performed by dividing the spectra into two regions, from 800 to 950 Å and from 920 to 1440 Å. The calibration was carried out in a similar manner to that described by Liu et al. (1995). The intensity ratios between the synthetic and observed spectra over the selected intervals and the intensity-weighted center wavelengths are fitted with a linear polynomial of fifth degree. The resulting polynomial is then used to calibrate the experimental spectra. Since accurate relative intensities of the $np\sigma\ ^1\Sigma_u^+$ and $np\pi\ ^1\Pi_u$ states have not been reported previously, several iterative rounds of calibration were made to assess the contribution from the $n \geq 4$ states. When the calibrated experimental and synthetic spectra are plotted together, emissions from the $n \geq 4$ states appeared as "extra peaks" or as enhanced intensities when not completely resolved. The "extra peaks" or enhanced intensities were further investigated by comparing their positions and assignment with the atlas list obtained from the following companion paper (Liu et al. 2000, hereafter Paper II) and from Roncin & Launay (1994). The start and end positions of the wavelength regions selected for calibration were adjusted based on assessment of the spectral positions and intensities of the "extra" feature. After the final calibrations were completed, the two calibration curves were smoothly joined in the 920–950 Å region. Figure 2 shows the combined relative sensitivity curve of the system.

The shape of the sensitivity curve in Figure 2 is primarily determined by the sensitivity of the channel electron multiplier and B_4C coated grating, which is blazed at 1200 Å. The quantum efficiency of the channeltron generally decreases with wavelength. Thus, the maximum sensitivity near 1060 Å and the decline from 1160 to 840 Å can be attributed to the increase in channeltron efficiency offset by the decrease in the grating sensitivity. Similarly, the decrease of the sensitivity between 1160 and 1200 Å is essentially caused by the decline in the quantum efficiency of the channeltron. The accelerated falloff above 1290 Å is due to the sensitivity drop of both channeltron and grating. However, the rise of the sensitivity from 840 to 810 Å is somewhat surprising and can be explained by the poor signal-to-noise ratio of the observed data, errors in calibration and model, or an anomaly of instrument.

It should be mentioned that the relative sensitivity curve in the 1140–1440 Å region Figure 2 is not comparable to that obtained by Liu et al. (1995) as the experimental setup is different between the two experiments.

The uncertainty of calibration is wavelength dependent.

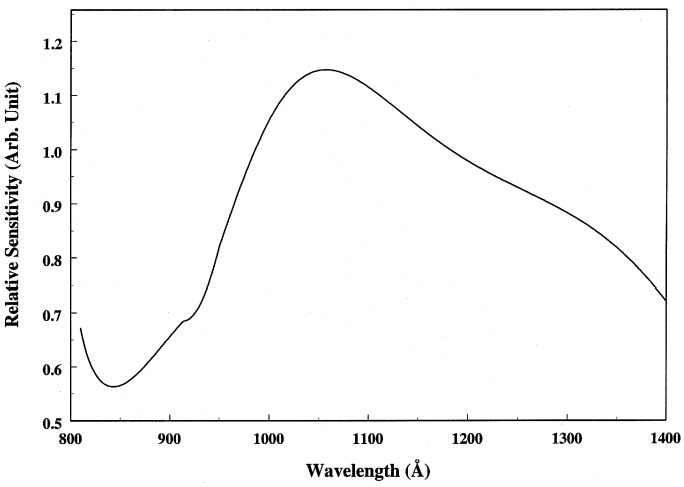

FIG. 2.—Instrumental sensitivity curve from 810 to 1400 Å as a function of wavelength. The sensitivity, S, is defined as the ratio of integrated experimental intensity to the integrated model intensity over the selected wavelength regions. Note that the S is set to 1.0 at $\sim$1177 Å.

The uncertainty for the 960–1400 Å region is estimated to be about 10%. Owing to the weakness of the emission intensities, the calibration uncertainty between 1400 and 1440 Å is slightly higher but is expected to be less than 15%. Similarly, the uncertainty in the 930–960 Å region is also expected to be less than 15% because of the interference from the high Rydberg states. However, the uncertainty in the 800–930 Å region is higher than 15% and can reach $\sim 30\%$ in certain cases.

4.3. *Spectral Analysis*

The overall experimental spectrum spans a region of 640 Å, from 800 Å to 1440 Å. Figure 3 shows the overplot of calibrated experimental and synthetic spectra at 100 eV from 900 Å to 1180 Å. The emission spectrum below 900 Å contains a large number of transitions from the $n \geq 4$ Rydberg states and will be presented in Paper II, together with the assignments. We note that the FUV emission spectra at 100 eV excitation energy in the 1140–1690 Å region obtained under slightly different experimental conditions has been presented elsewhere (Liu et al. 1995). The overall agreement between the observed and synthetic spectra in the 1140–1400 Å region of the present study is slightly better than that shown by Liu et al. (1995). The slight improvement over the 1995 data is due to the utilization of the continuum profiles of Abgrall et al. (1997), instead of the rotationless Stephens & Dalgarno (1972) continuum profiles and consideration of both isotropic and anisotropic rotational channels in $E, F\ ^1\Sigma_g^+ - X\ ^1\Sigma_g^+$ excitation (Abgrall et al. 2000). This results in a significant improvement for certain $B\ ^1\Sigma_u^+ - X\ ^1\Sigma_g^+$ emissions from the $J_j = 3$ and 4 levels that are strongly enhanced by $E, F\ ^1\Sigma_g^+ - B\ ^1\Sigma_u^+$ cascade transitions. In Figure 3, we allow a 40 Å overlap with the previous spectra in the 1140–1180 Å region because the previous synthetic spectrum for the $B'\ ^1\Sigma_u^+ - X\ ^1\Sigma_g^+$ transition was generated with band transition probabilities with certain scaling factors and because the diverter mirror used in the previous experiment had very significant variation in reflectivity in the region and introduced fairly large uncertainties in calibration. Calibrated

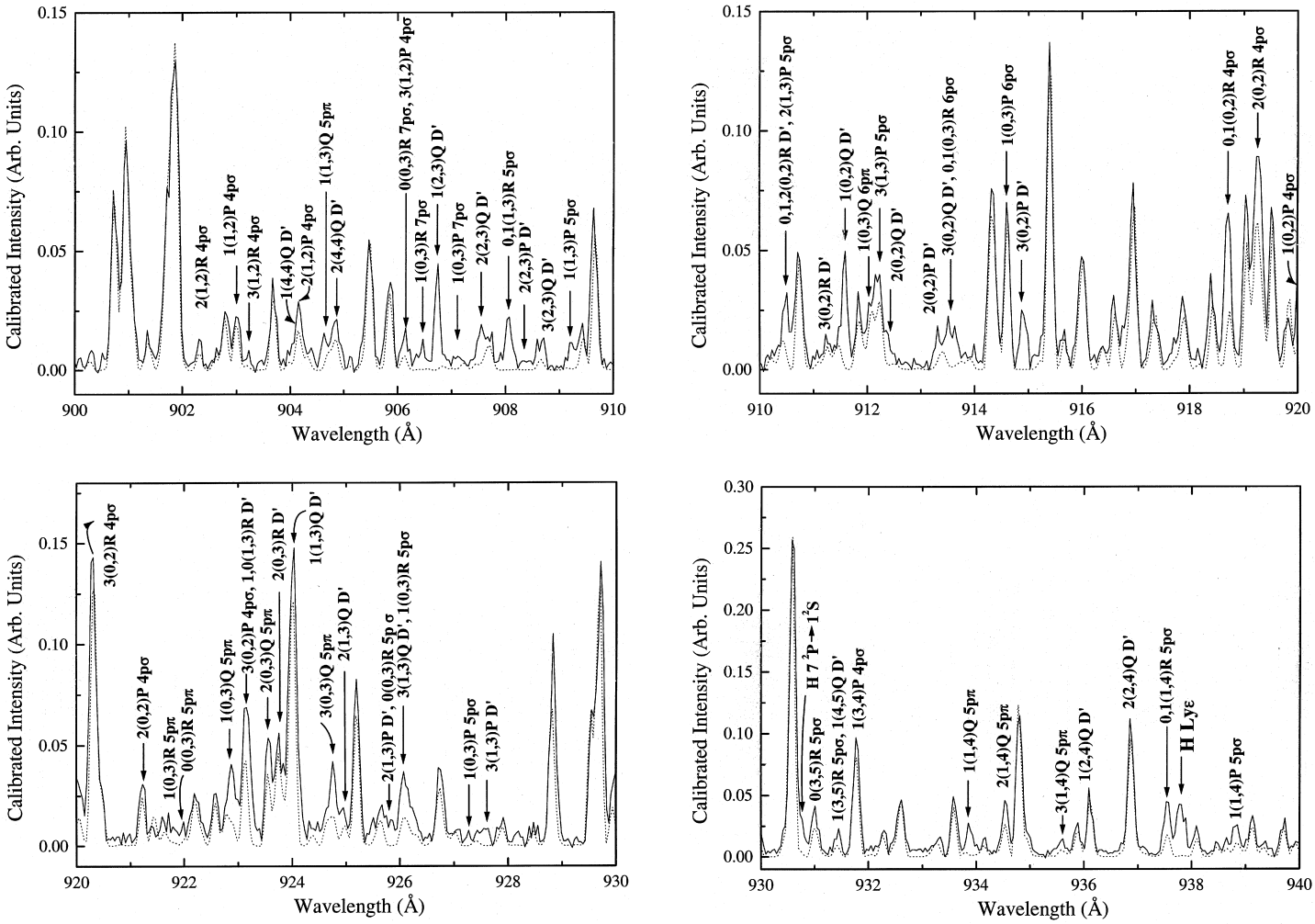

FIG. 3.—Comparison between the experimental (*solid lines*) and synthetic (*dotted lines*) spectra obtained at 300 K, 100 eV excitation energy, and 0.115 Å (FWHM) resolution. Experimental spectrum has been corrected for the instrumental sensitivity variation as described in the text. The uncertainty of experimental intensity calibration in 900–930 Å and 930–1180 Å regions is estimated to be less than 15% and 10%, respectively. The synthetic spectrum is calculated from the $B\ ^1\Sigma^+{}_u - X\ ^1\Sigma^+{}_g$, $C\ ^1\Pi_u - X\ ^1\Sigma^+{}_g$, $B'\ ^1\Sigma^+{}_u - X\ ^1\Sigma^+{}_g$, and $D\ ^1\Pi_u - X\ ^1\Sigma^+{}_g$ transition probabilities of Abgrall et al. (1993a, 1993b, 1993c, 1994) and excitation function of Liu et al. (1998). The self-absorption of the model spectrum has been considered by adopting a foreground H_2 column density of 2×10^{13} cm^{-2} (see text). The synthetic spectrum has been convoluted with a triangular instrumental line profile with 0.115 Å resolution. Atomic hydrogen Lyman series emission and major emission of molecular hydrogen originated from higher (i.e., $n > 4$) Rydberg states, both of which are not considered by the model, are indicated.

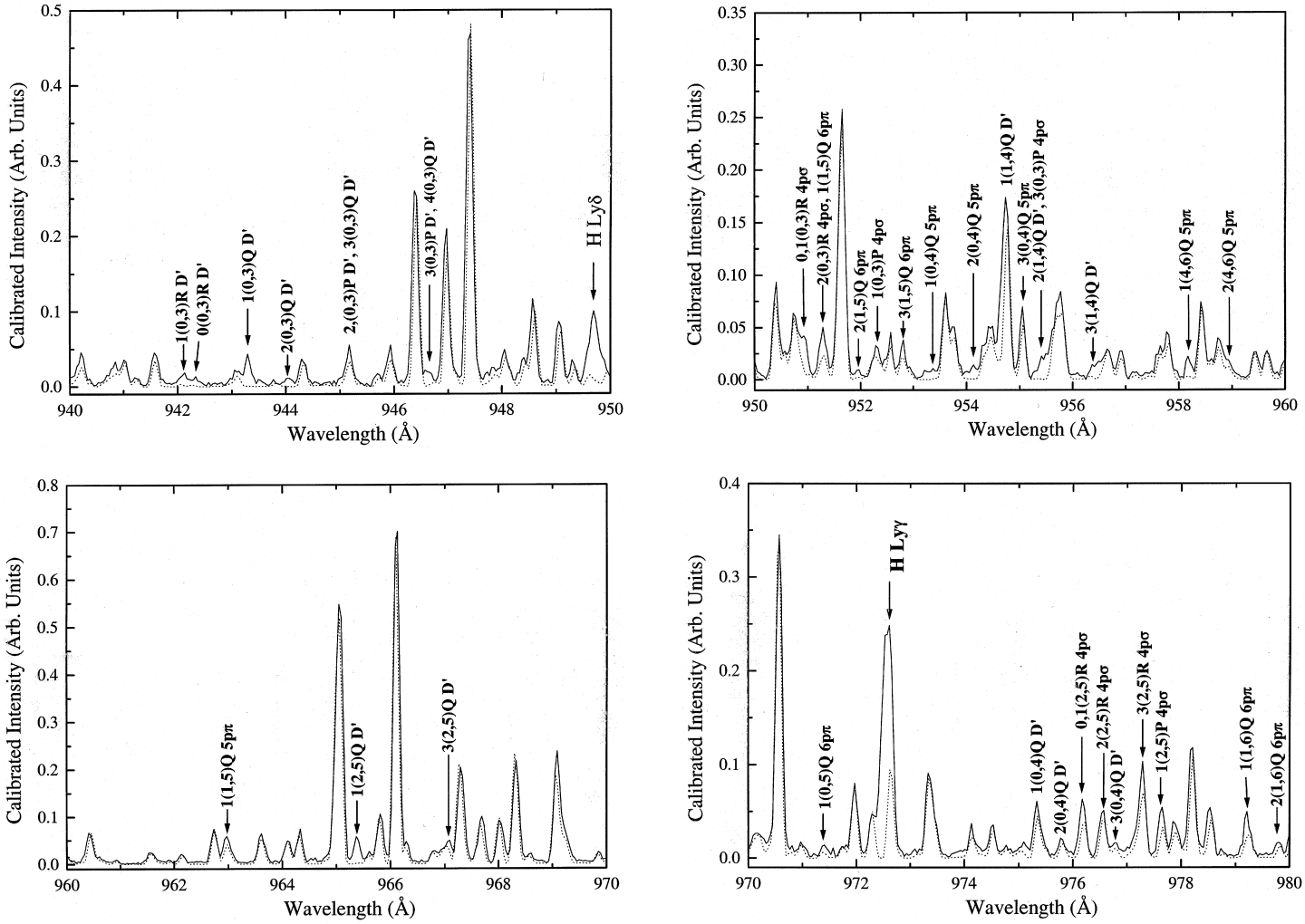

FIG. 3.—*Continued*

experimental and model spectra shown in Figure 3 can be obtained in electronic form.[3]

It should be stated again that the present model considers only the $B\ ^1\Sigma_u^+ - X\ ^1\Sigma_g^+$, $C\ ^1\Pi_u - X\ ^1\Sigma_g^+$, $B'\ ^1\Sigma_u^+ - X\ ^1\Sigma_g^+$, and $D\ ^1\Pi_u - X\ ^1\Sigma_g^+$ transitions. As a result, emissions from the higher ($n \geq 4$) Rydberg states and from atomic hydrogen Lyman $n\ ^2P_{3/2,1/2} - ^2S_{1/2}$ series appear as either additional lines or extra intensities when not fully resolved in the observed spectra. Transitions from the atomic fragment or from the higher Rydberg states of H_2 are marked with appropriate symbols in Figure 3. The assignments of the higher Rydberg emission are indicated when the labeling does not cause too much congestion. Except for these additional lines and a few discrepancies discussed below, the agreement between the experimental and model spectra is very good.

We now discuss self-absorption for the resonance transitions of the Werner and Lyman band systems. For the $(v_j,0)$-type transitions, the rotational dependence of the transition dipole matrix element is small. So, the band transition probabilities, $A_{P(J+1)} + A_{R(J-1)}$, can be considered to be independent of J. In the absence of a local perturbation, the line transition probabilities, $A(v_j, v_i; J_j, J_i)$, in equation (2b) can be approximated by a product of Hönl-London factors and band transition probabilities. We can rewrite the extinction coefficient of equation (2b) as

$$\epsilon^{\mathrm{W}}_{P(J)} = \frac{1.427 \times 10^{-7}}{\nu^3} \frac{J-1}{2J+1} A(v_j, 0)\,, \tag{6a}$$

$$\epsilon^{\mathrm{W}}_{Q(J)} = \frac{1.427 \times 10^{-7}}{\nu^3} A(v_j, 0)\,, \tag{6b}$$

$$\epsilon^{\mathrm{W}}_{R(J)} = \frac{1.427 \times 10^{-7}}{\nu^3} \frac{J+2}{2J+1} A(v_j, 0)\,, \tag{6c}$$

$$\epsilon^{\mathrm{L}}_{P(J)} = \frac{1.427 \times 10^{-7}}{\nu^3} \frac{J}{2J+1} A(v_j, 0)\,, \tag{6d}$$

$$\epsilon^{\mathrm{L}}_{R(J)} = \frac{1.427 \times 10^{-7}}{\nu^3} \frac{J+1}{2J+1} A(v_j, 0)\,, \tag{6e}$$

where the superscripts W and L denote the Werner and Lyman transitions, J refers to the rotational quantum number of the ground state (i.e., J_i), and $A(v_j, 0)$ is the band transition probability, which is assumed to be independent of J_i and J_j.

At 300 K, the fractional population at $J_i = 0$, 1, 2, 3, and 4 levels of the ground state are 12.88%, 65.65%, 11.77%, 9.17%, and 0.43%, respectively. Thus equations (2a) and (6a)–(6e) show that the strongest resonance attenuation

[3] Contact X. Liu; email: Xianming@rcf.usc.edu.

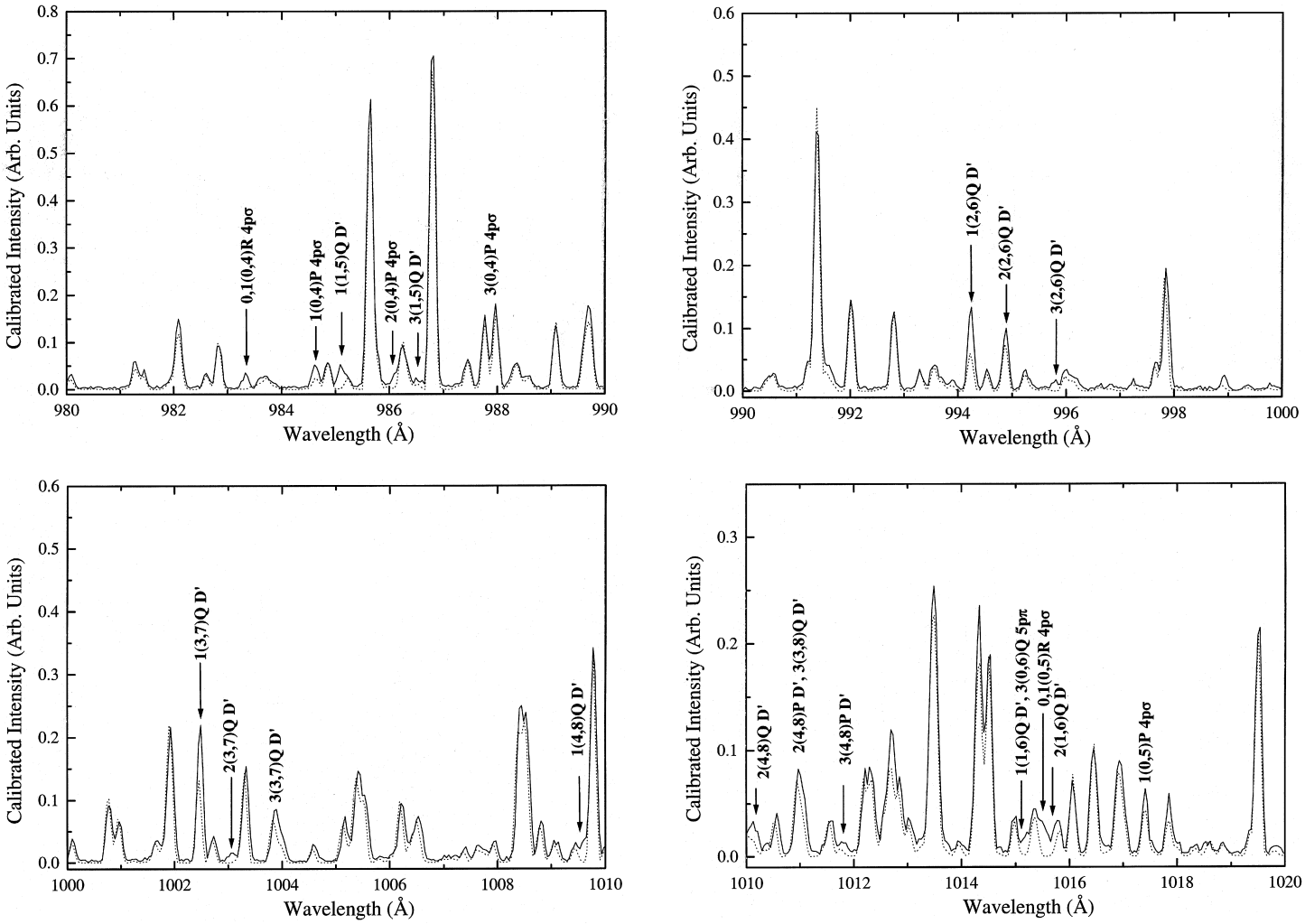

FIG. 3.—*Continued*

occurs at the $Q(1)$ and the $R(1)$ transitions of the Werner band and $R(1)$ transition of the Lyman band. In the absence of perturbations, equations (6b) and (6c) indicate that the attenuation factors of $R(1)$ and $Q(1)$ are approximately equal. Owing to a factor of 5 difference in population between $J = 0$ and 1 levels, the attenuation factor of $R(0)$ transitions for both Lyman and Werner bands are smaller than their $R(1)$ counterparts, in spite of a larger extinction coefficient for $R(0)$. It should also be noted that the optical depth, $\epsilon_i \zeta_i$, of the $P(2)$, $P(3)$, and $R(2)$ transitions of the Werner band system are about 28, 25, and 7 times smaller, respectively, than that of the $Q(1)$ transition. At the foreground column density near 2×10^{13} cm^{-2}, the attenuation values for the resonance transitions involved the $J_i \geq 2$ levels are negligibly small. For the ($v_j = 0$–4, 0) resonance band of the Werner system, the $Q(1)$ transition shows as a strong emission line. The $R(0)$ and $R(1)$ emissions are generally not resolved at the present resolution and are located at ~ 1 Å on the blue side of the $Q(1)$ emission. The $P(3)$ line, whose intensity is slightly weaker than that of $R(0)/R(1)$ emission, appears at 4–4.5 Å on the red side of the $Q(1)$ transition. The relative intensities of the $Q(1)$ and $P(3)$ transitions are therefore very sensitive to the foreground column density and are used to determine the foreground column density. When the $P(3)$ line overlaps with other strong transitions, the relative intensities between $Q(1)$ and $R(0)/R(1)$ rotational lines are also used. The column density is adjusted until the relative intensities between the observed and synthesized values for the $R(0)/R(1)$, $Q(1)$, and $P(3)$ transitions of the ($v_C = 0$–4, 0) bands are matched. The calculated line transition probabilities, $A(v_j, v_i; J_j, J_i)$, are used for computation of optical depth. The agreement between the strong lines in the 929–935 Å, 946–952 Å, 964–971 Å, 985–991.8 Å, and 1008–1015 Å regions in Figure 3, which approximately correspond to the (4, 0), (3, 0), (2, 0), (1, 0), and (0, 0) bands the of Werner system, respectively, shows the consistency and relative accuracy of the simple self-absorption model and foreground effective column density.

It is interesting to note the good agreement between the observed and model intensities for the emissions originating from the $J_j = 1$, 2, and 3 levels for $v_j = 14$ of the $B\,^1\Sigma_u^+$ state and the $v_j = 3$ level of the $C\,^1\Pi_u^+$ state. As mentioned earlier, these levels are strongly coupled. The $J_j = 1$ levels, for instance, have about a 69%/31% mixing ratio according to the calculation of Abgrall & Roueff (1989).[4] As a result of

[4] The square of the eigencoefficients for the $J_j = 1$ and $v_j = 14$ level of the $B\,^1\Sigma_u^+$ state obtained by a more recent calculation of Abgrall et al. (2000) are 0.694, 0.306, 5.39×10^{-5}, and 3.38×10^{-6}, respectively, for the $B\,^1\Sigma_u^+$, $C\,^1\Pi_u^+$, $B'\,^1\Sigma_u^+$, and $D\,^1\Pi_u^+$ Born-Oppenheimer states. The use of the new coefficients, however, will not introduce any significant changes in the results presented here.

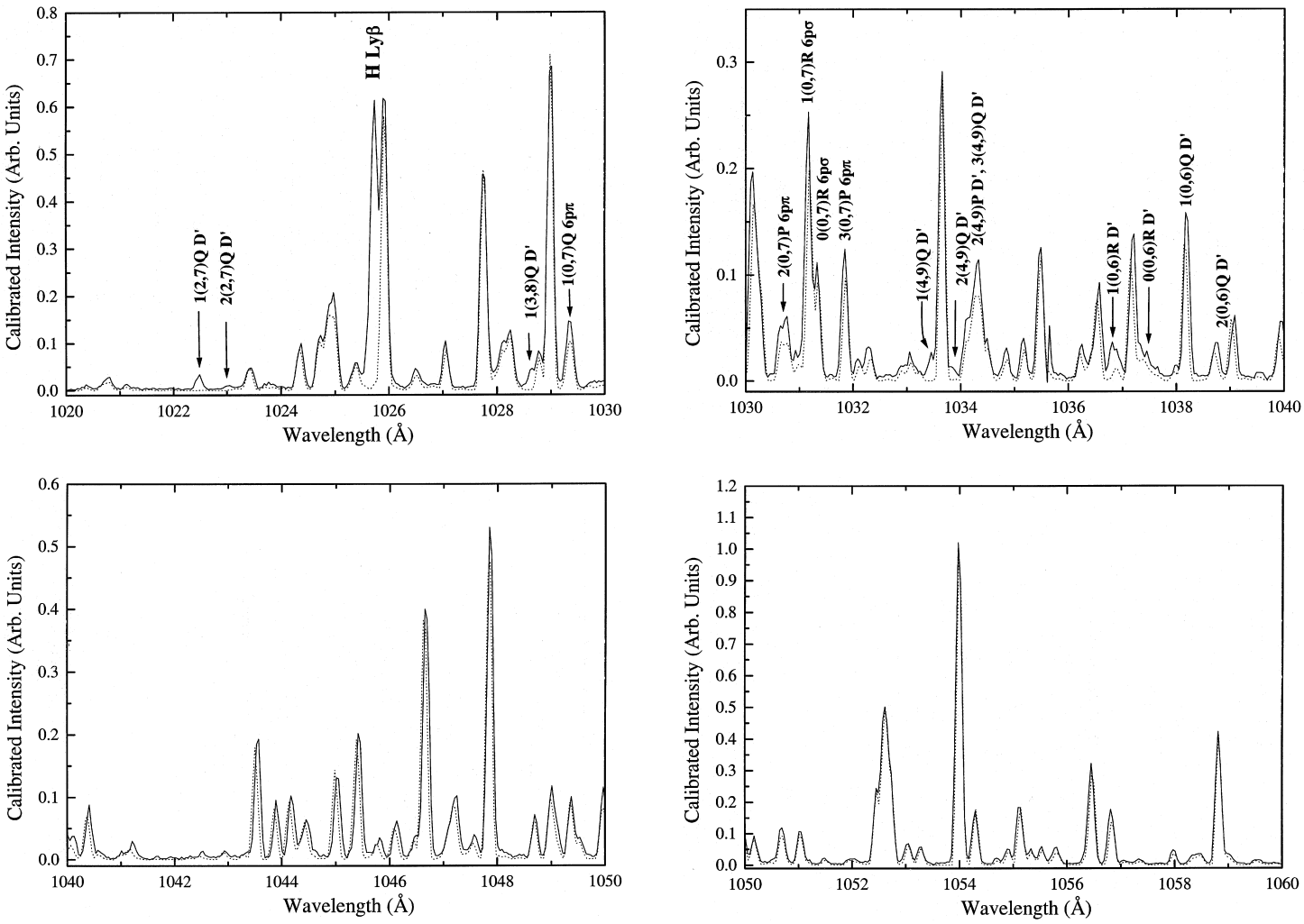

FIG. 3.—*Continued*

the coupling, emission intensities from these levels deviate significantly from those of unperturbed levels. At a temperature of 300 K and an excitation energy of 100 eV, the intensity of the $R(0)$ line of the (14, 0) Lyman band emission drops by 92% while those of the $R(1)$ and R(2) transitions of the same band increase by almost 700% and 400%, respectively (Liu et al. 1995). The 700% increase in the intensity makes the R(1) transition appear as a strong line near the 947 Å region of the $B\ ^1\Sigma_u^+$–$X\ ^1\Sigma_g^+$ model spectrum in Figure 1. The perturbation also changes the intensities of the (3, 0) Werner band emissions. For instance, while the intensity of the $R(0)$ line increases by $\sim$26%, those of the $P(2)$, $R(1)$, $P(3)$, $R(2)$, and $P(4)$ transitions decrease by 83%–8%. Similar intensity deviations also occur at (14, 2)/(3, 2) (1027 $\pm$ 4 Å), (14, 4)/(3, 4) (1108 $\pm$ 4 Å), (14, 6)/(3, 6) (1090 $\pm$ 4 Å), and other bands. The good agreement in relative intensity between experiment and model in these regions shows the accuracy of the calculation of Abgrall et al. (1989, 1993a, 1993b, 1993c, 1994) and Abgrall & Roueff (1989).

The $J_j = 3$ and 4 levels of $v_j = 2$ of the $C\ ^1\Pi_u^+$ state and $v_j = 12$ of the $B\ ^1\Sigma_u^+$ state are also strongly coupled. The effect of perturbation on the individual transition intensity is comparable to or slightly weaker than that of $v_j = 14$ of the $B\ ^1\Sigma_u^+$ state and $v_j = 3$ of the $C\ ^1\Pi_u^+$ state. However, its effect on overall emission intensities is significantly weaker because the population at $J_i \geq 2$ level is only 22.4%. Nevertheless, good intensity agreement is also achieved between the experimental and synthetic spectra for emission from $v_j = 2$ of the $C\ ^1\Pi_u^+$ state and $v_j = 12$ of the $B\ ^1\Sigma_u^+$ state.

A number of significant discrepancies in the experimental and model spectral intensities are also observed. The most noticeable differences involve emissions from the $J_j = 1$ and 2 levels for $v_j = 4$ of the $B'\ ^1\Sigma_u^+$ state. For instance, the model overestimates the intensities for the $R(1)$ and $P(3)$ lines of the (4, 0) $B'\ ^1\Sigma_u^+$–$X\ ^1\Sigma_g^+$ band by $\sim$70%, while it underestimates those of the $R(0)$ and $P(2)$ lines by $\sim$50%. The discrepancy between the model and observed emission intensities from the $J_j = 1$ and 2 levels for $v_j = 4$ of the $B'\ ^1\Sigma_u^+$ state is caused by the perturbation between the $v_j = 4$ level of the $B'\ ^1\Sigma_u^+$ state and the $v_j = 0$ level of the $B''\ ^1\Sigma_u^+$ state, which has not been considered in the calculation of Abgrall et al. (1994). It is worth noting that the energy value calculated by Abgrall et al. for the $J_j = 1$ and $v_j = 4$ level of the $B'\ ^1\Sigma_u^+$ state differs from the experimental value by more than 5 cm^{-1}. In addition to disagreement at the $J_j = 1$ and 2 levels for $v_j = 4$ of the $B'\ ^1\Sigma_u^+$ state, the present study also indicates that the calculated emission intensities from the $v_j = 0$ and 1 levels are generally 20%–30% weaker than the observed intensities.

4.4. *Emission Cross Sections and Nonradiative Yields*

Once the experimental spectra are calibrated, the emission cross sections of the $B''\ ^1\Sigma_u^+$, $D'\ ^1\Pi_u$, $D''\ ^1\Pi_u$, or higher

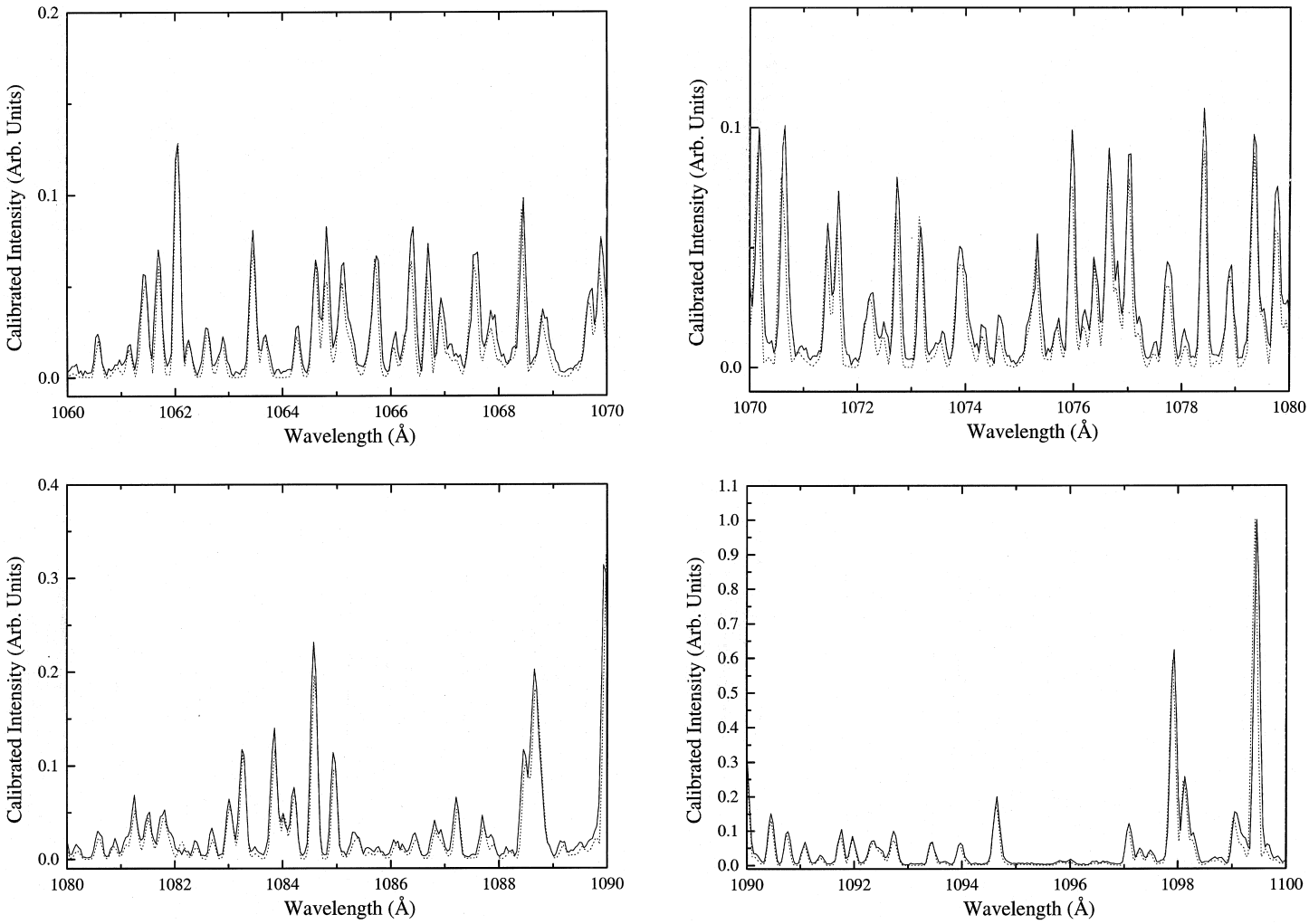

FIG. 3.—*Continued*

states can be obtained from the relative emission intensity measurements. Nonradiative yields can also be inferred by comparing emission and excitation cross sections.

4.4.1. *Emission Cross Sections*

As mentioned in § 4.1.1, the largest attenuation for the $B'\ ^1\Sigma_u^+$–$X\ ^1\Sigma_g^+$ and $D\ ^1\Pi_u$–$X\ ^1\Sigma_g^+$ emission intensities are only 1.8% and 2.7%, respectively, at the foreground column density of 2.0×10^{13} cm^{-2}. Hence, all the transitions of the $B'\ ^1\Sigma_u^+$–$X\ ^1\Sigma_g^+$ and $D\ ^1\Pi_u$–$X\ ^1\Sigma_g^+$ systems can be considered as optically thin.

Relative intensities from various rovibrational levels of the $np\sigma\ ^1\Sigma_u^+$ and $np\pi\ ^1\Pi_u$ states with $n \geq 3$ were measured from the calibrated observed spectra to obtain the relative emission cross sections. The relative intensity measurement was performed by numerically integrating the areas beneath proper spectral peaks. Owing to spectral congestion, emission from one band may overlap with that from another. Different emission intensity–partitioning procedures were used, depending on the electronic band system of the overlapping transitions. If the overlapping peak involves only transitions from the $B\ ^1\Sigma_u^+$, $C\ ^1\Pi_u$, $B'\ ^1\Sigma_u^+$, and $D\ ^1\Pi_u$ states, the emission intensities for different transitions were partitioned according to the model output. If the overlapping peak consists of one transition from an $n \geq 4$ state and a number of transitions from $n \leq 3$ states, the intensity difference between calibrated and synthetic spectra was partitioned to the $n \geq 4$ state and the remaining intensities distributed according to the model output. In partitioning emission intensities involving the high Rydberg state, we followed the spectral assignments of Roncin & Launay (1994) and assignments presented in Paper II. If the spectral peak consists of two or more transitions from the $n \geq 4$ states, the partition by model is not possible. In limited cases, it is possible to predict the transition from the $n \geq 4$ state that makes the predominant contribution to the observed intensities. For example, if two emission lines such as $Q(1)$ and $P(4)$ of the proper $n \geq 4$ states are involved, the observed intensity would be partitioned to the $Q(1)$ transition on the basis of the large population difference between the $J_i = 1$ and $J_i = 2$ (or 4) levels and the possibility of predissociation of the $^1\Sigma_u^+$ or $^1\Pi_u^+$ states. However, if it was impossible to predict which transition from the $n \geq 4$ state makes the major contribution, the relative intensities would not be counted. Similarly, if a transition observed in the present work was not observed by Roncin and Launay or was observed but not assigned, the emission cross section of the transition would not be counted.

The absolute emission cross sections are established by using the absolute emission cross sections of Lyman and Werner transitions in the 1098.7–1100.0 Å region. The $1(0, 2)QW$ emission contributes about 74.8% of intensities

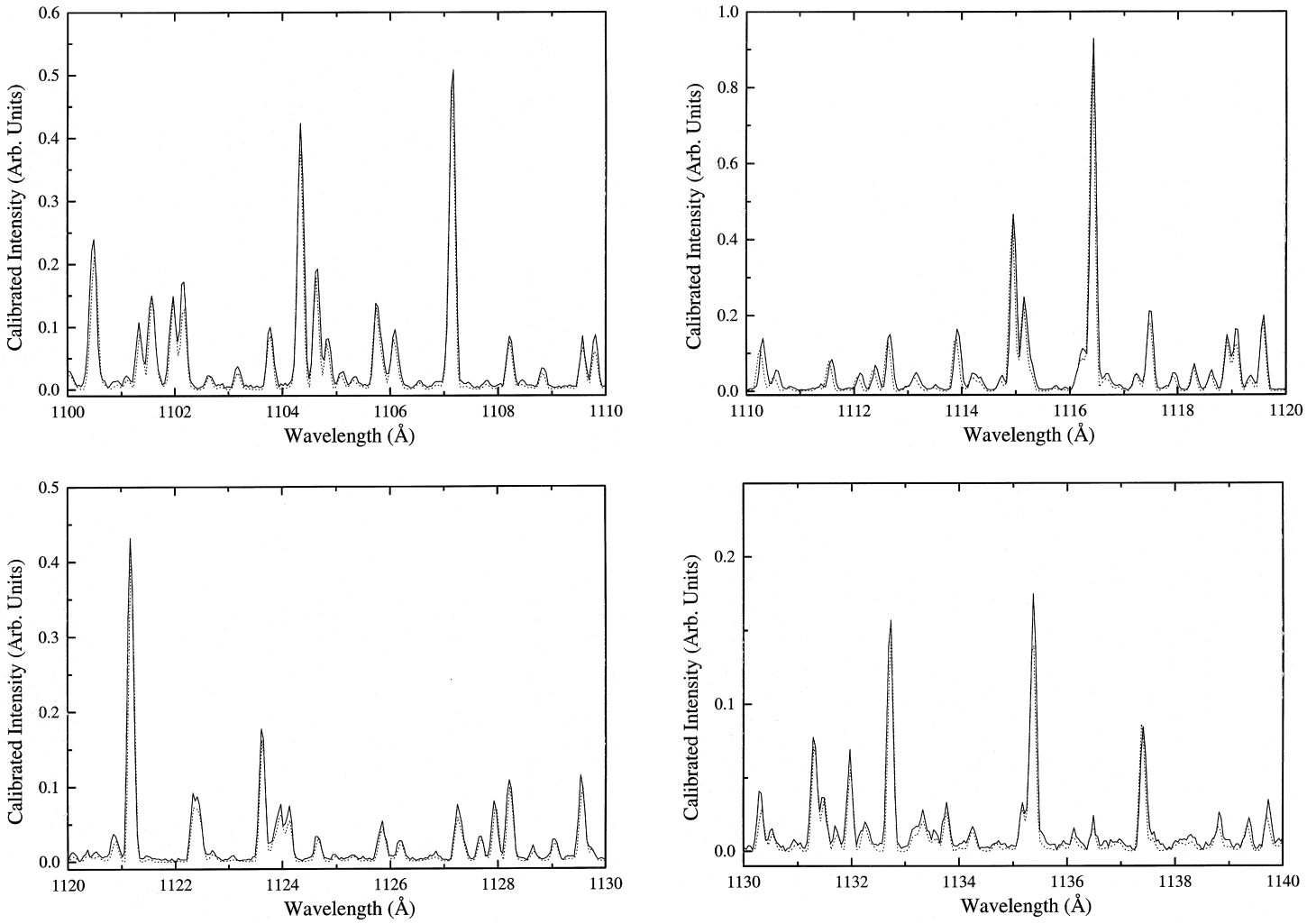

FIG. 3.—*Continued*

for the region at 100 eV and 300 K. Other weak but significant transitions are 1(7, 6)*RW* (1.2%), 1(4, 1)*PL* (10.7%), 3(0, 2)*RW* (3.1%), 1(11, 3)*PL* (1.9%), 2(4, 1)*RL* (1.8%), 1(7, 6)*QW* (2.4%), 5(5, 1)*PL* (1.1%), and 3(1, 0)*PL* (1.1%). The absolute emission cross sections for the transitions between 1098.7 and 1100.0 Å region can be calculated from the work of Liu et al. (1998). The total emission cross section for the transitions in this region is 5.45×10^{-19} cm^2. The measured absolute emission cross section for individual line are summed over proper v_j and J_j to obtain vibrational and electronic band emission cross sections, which are listed in Tables 1 and 2, respectively.

Since certain overlapping emission lines from higher Rydberg states ($n \geq 4$) are not summed, the vibrational band emission cross sections in Table 1 and electronic band emission cross sections in Table 2, in general, should be considered as lower limits. Other errors, such as calibration and numerical integration, however, should also be considered. The third column of Table 1 lists vibrational band excitation cross sections of the $B'\ ^1\Sigma_u^+$ and $D\ ^1\Pi_u$ states. If the errors in calibration, integration, and partitioning were negligible and the $B'\ ^1\Sigma_u^+ - X\ ^1\Sigma_g^+$ and $D\ ^1\Pi_u - X\ ^1\Sigma_g^+$ transition probabilities are sufficiently accurate, the vibrational band cross sections listed in the second and third columns would have been identical. Thus, the difference between the second and third columns is an indicator of the combined calibration, integration, and partitioning errors. The largest difference, 50%, occurred at $v_j = 7$ of the $D\ ^1\Pi_u^-$ state, suggesting that the error in the experimental vibrational band cross sections is $\sim$50%. For the weaker $B''\ ^1\Sigma_u^+ - X\ ^1\Sigma_g^+$, $D'\ ^1\Pi_u - X\ ^1\Sigma_g^+$, and $D''\ ^1\Pi_u - X\ ^1\Sigma_g^+$ transitions, the error could approach 100%. Owing to the possibilities of undercounting or overcounting of intensities in the partition of the overlapping spectral transitions, the large error in the vibrational band cross section for the weak transition is understandable. The measurement error at the electronic band cross section level, however, is expected to be smaller owing to the diminishing effect of undercounting or overcounting intensities and the trend of cancellation in numerical integration error. For instance, Table 2 shows that the measurement error on an electronic band system basis is about 10%. Again, for the higher Rydberg states, the error can be a few times higher.

4.4.2. *Nonradiative Yields*

The predissociation yield of a rotational level can be defined as the ratio of the predissociation rate to the total decay rate for that level. For a steady state system, the total decay rate is equal to the excitation rate. Since collision deactivation is negligible in this study, the sum of predissociation and autoionization rate equals the difference between the excitation and radiative emission rates. For an

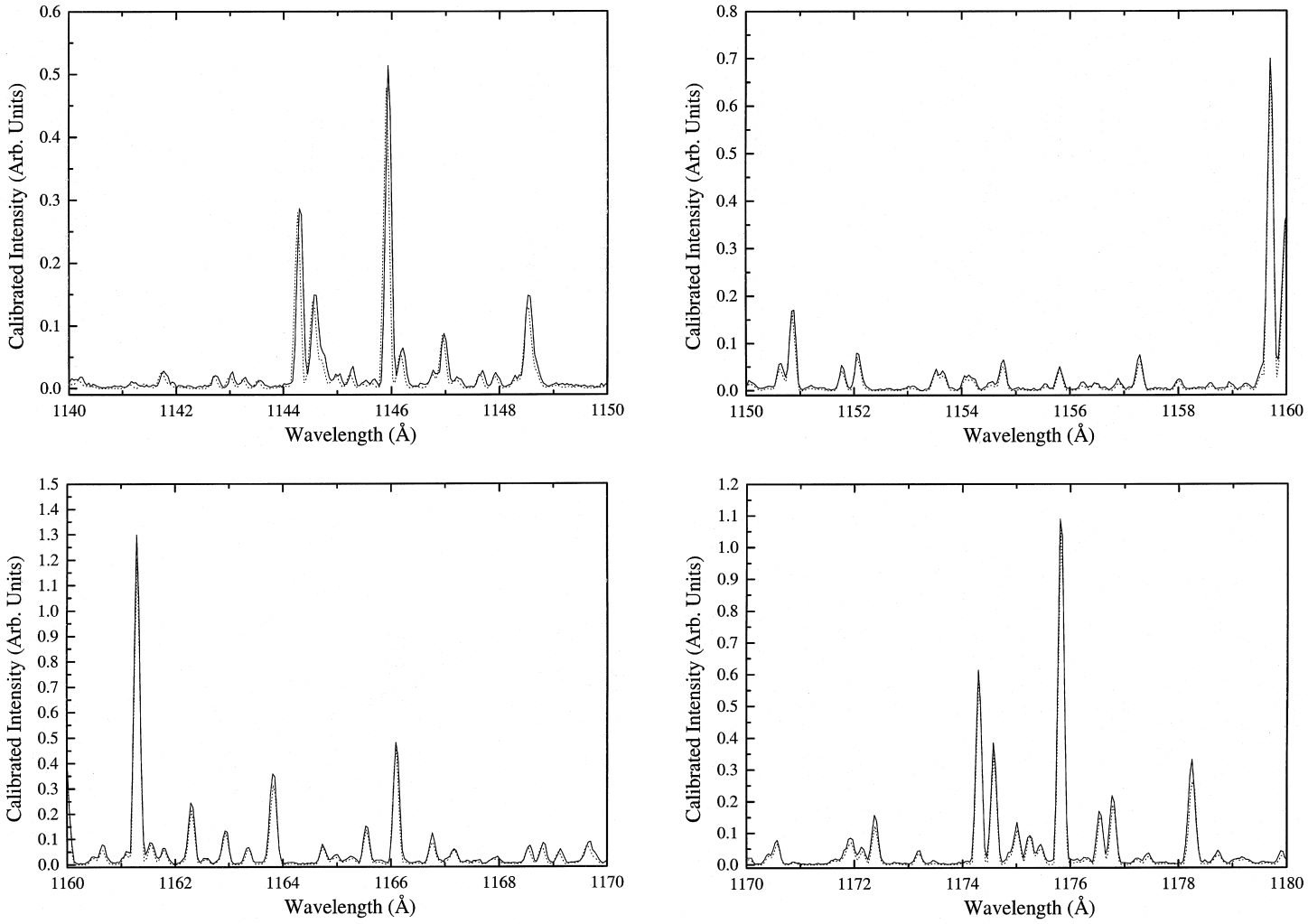

FIG. 3.—*Continued*

electronic band system, the sum of predissociation and autoionization yield is equal to the ratio of the difference between the excitation and emission cross sections to the excitation cross section. If the excitation cross section is known, the nonradiative yield can be obtained from the measured emission cross section.

The $B'\ ^1\Sigma_u^+ - X\ ^1\Sigma_g^+$ excitation process consists of both discrete and continuum transitions. Excitation to the discrete levels gives rise to $B'\ ^1\Sigma_u^+ - X\ ^1\Sigma_g^+$ emissions, while excitation into the continuum levels results in dissociation. The dissociation yield of the $B'\ ^1\Sigma_u^+$ state is equal to the excitation cross section of the continuum levels divided by the total (discrete + continuum) cross section. The emission cross section of the $B'\ ^1\Sigma_u^+$ state is measured to be 2.1×10^{-18} cm^2. The emission cross section equals the excitation cross section to the discrete levels of the $B'\ ^1\Sigma_u^+$ state. If the dependence of electronic transition moment on internuclear distance and the couplings between the $B'\ ^1\Sigma_u^+$ and other states are neglected, the excitation cross section to the continuum levels can be estimated from the discrete and continuum portions of Frank-Condon factors, which can be calculated from the adjusted adiabatic potential of Abgrall et al. (1994). For the $P(1)$ of $(v_j, 0)$ excitations, for example, the sums of the discrete and continuum Frank-Condon factors are 0.55 and 0.45, respectively (see the seventh column of the Table 1). Thus, the excitation cross section to the continuum level of the $B'\ ^1\Sigma_u^+$ state is approximately $0.45 \times 2.1 \times 10^{-18}/0.55$ or 1.7×10^{-18} cm^2, and the total excitation cross section is approximately 3.8×10^{-18} cm^2. Alternatively, the cross section can be estimated from the discrete and continuum parts of the oscillator strength. For the $P(1)$ transition, the total oscillator strengths for the discrete and continuum excitations are 0.01117 and 0.00829, respectively. The continuum and total cross sections of the $B'\ ^1\Sigma_u^+$ state are 1.6×10^{-18} and 3.7×10^{-18} cm^2. The dissociation yield of the $B'\ ^1\Sigma_u^+ - X\ ^1\Sigma_g^+$ band systems is, therefore, 43%–45%.

It is interesting to compare the calculated Frank-Condon factors, $q_{v,0}$(cal), with the experimentally determined relative Frank-Condon factors. At 300 K, all the H_2 molecules are in the $v_i = 0$ level. In addition, the effect of the difference in the threshold energy of excitations is negligible at 100 eV excitation energy. Under these conditions, the vibrational band emission cross section, $\sigma_{em}(v)$, is proportional to the Frank-Condon factor, $q_{v,0}$(exp). We have

$$q_{v,0}(\text{exp}) = \frac{\sigma_{em}(v)}{\sum_{v=0}^{9} \sigma_{em}(v)} \sum_{v=0}^{9} q_{v,0}(\text{exp}) \, . \qquad (7)$$

If we require the sum of the discrete $q_{v,0}$(exp) to be equal to the sum of the discrete $q_{v,0}$(cal) (which, in turn, equals 0.55), we can calculate the individual $q_{v,0}$ (exp.). These numbers

TABLE 1

CROSS SECTIONS OF THE $B'\ ^1\Sigma_u^+$, $D\ ^1\Pi_u$, $B''\ ^1\Sigma_u^+$, $D'\ ^1\Pi_u$, AND $D''\ ^1\Pi_u$ STATES

State	v_j	σ_{em} (exp)[a,b]	σ_{ex} (mod)[a,c]	σ_{ex} (est)[a,d]	σ (nonrad)[a]	FC Factor $q_{v,0}$(cal)[e]	FC Factor $q_{v,0}$(exp)[f]
$B'\ ^1\Sigma_u^+$	0	2.27	1.77	2.27	0.0	0.049	0.06
	1	4.89	3.86	4.89	0.0	0.099	0.13
	2	5.07	4.43	5.07	0.0	0.12	0.14
	3	3.56	3.48	3.56	0.0	0.12	0.10
	4	3.60	3.72	3.60	0.0	0.094	0.10
	5	1.07	1.45	1.07	0.0	0.054	0.03
	6–9	~0.1	0.31	~0.1	~0.0	0.016	~0.0
	Continuum[g]	...	...	~20	~20	0.45	...
$D\ ^1\Pi_u^-$	0	1.79	2.49	1.79	0.0	0.099	0.10
	1	3.66	4.08	3.66	0.0	0.17	0.21
	2	4.36	4.02	4.36	0.0	0.18	0.25
	3	2.32	3.24	2.32	0.0	0.15	0.13
	4	2.04	2.38	2.04	0.0	0.12	0.12
	5	1.22	1.65	1.22	0.0	0.084	0.07
	6	0.87	1.10	0.87	0.0	0.059	0.05
	7	0.37	0.73	0.37	0.0	0.040	0.02
	8	0.48	0.48	0.48	0.0	0.027	0.03
	9	0.22	0.32	0.22	0.0	0.019	0.01
	10–14	~0.3	0.54	~0.3	0.0	0.031	~0.02
$D\ ^1\Pi_u^+$	0	2.20	2.58	2.20	0.0	0.099	...
	1	4.70	5.18	4.70	0.0	0.17	...
	2	3.90	4.19	3.90	0.0	0.18	...
	3–14	0.0	...	~13	~13	0.51	
$D'\ ^1\Pi_u^-$	0–6	~5.34	...	>5.34	0.0	0.861	...
$D'\ ^1\Pi_u^+$	0	~0.95	...	~0.95	0.0	0.095	...
	1–5	~0.06	...	>6.3	>6.2	0.71	...
$B''\ ^1\Sigma_u^+$	0	1.55	...	1.55	0.0	...	...
$D''\ ^1\Pi_u^-$	0	0.59	...	0.59	0.0	...	...

[a] Unit is 10^{-19} cm^2. σ_{ex} and σ_{em} denote excitation and emission cross sections, respectively.
[b] Measured in the present work.
[c] Computed by using Lyman and Werner shape function with the calculated oscillator strength.
[d] Estimated by the present work. See text.
[e] Calculated in the present work.
[f] Experimental Frank-Condon factor is calculated by $q_{v,0} = \sigma_{em}(v)/\Sigma\sigma_{em}(v)$, with the summation of $q_{v,0}$ over the discrete levels fixed to the calculated value.
[g] See text.

TABLE 2

BAND SYSTEM CROSS SECTIONS AND NONRADIATIVE YIELDS OF H_2

State	Present σ_{ex}[a]	Present σ_{em}[a,b]	Previous σ_{ex}[a,c]	Previous σ_{em}[a,c]	Nonradiative Yield (η) (%)
$B\ ^1\Sigma_u^+$	262 [d]	262[d]	267	267	0.0
$C\ ^1\Pi_u$	241 [d]	241[d]	278	278	0.0
$B'\ ^1\Sigma_u^+$ [e]	21	21 (22)	82	82	0.0
$B'\ ^1\Sigma_u^+$ [f]	38	21 (22)	...	...	44
$B''\ ^1\Sigma_u^+$	>4	1.6	17	0.8	>40
$D\ ^1\Pi_u^+$	24	11 (12)	...	...	54
$D\ ^1\Pi_u^-$	18	18 (21)	...	...	0.0
$D\ ^1\Pi_u$	41	28 (33)	67	47	32
$D'\ ^1\Pi_u^+$	7.1	1.0	...	...	86
$D'\ ^1\Pi_u^-$	5.3	5.3	...	...	0.0
$D'\ ^1\Pi_u$	12	6.3	34	19	49
$D''\ ^1\Pi_u$	>0.59	0.59	...	...	...

[a] Unit is 10^{-19} cm^2. σ_{ex} and σ_{em} denote excitation and emission cross sections, respectively.
[b] Numbers in parentheses are obtained by using Lyman and Werner shape function with the calculated oscillator strength.
[c] From Ajello et al. 1988.
[d] From Liu et al. 1998.
[e] Excluding excitations to the continuum levels of the $B'\ ^1\Sigma_u^+$ state.
[f] Including excitations to both discrete and continuum levels of the $B'\ ^1\Sigma_u^+$ state.

are listed in the last column of Table 1. The agreement between the $q_{v,0}$ (exp) and $q_{v,0}$ (cal) is reasonable good for the $B'\ ^1\Sigma_u^+$–$X\ ^1\Sigma_g^+$ state.

The predissociation yield of the $D\ ^1\Pi_u$–$X\ ^1\Sigma_g^+$ band system can be estimated from the fact that the $v_j \geq 3$ levels of the $D\ ^1\Pi_u^+$ state predissociate completely while the other levels do not predissociate (§ 4.1.3).[5] If the excitation energy is not too low so that the effect of the difference in the threshold energies, E_{ij}, of equation (4) can be neglected, the contribution of each excitation to the total cross section of equation (5) is proportional to the absorption oscillator strength, f_{ij}, and fractional population, N_i/N_t. In absence of the $^1\Sigma_u^+$–$^1\Pi_u^+$ perturbations and rotational dependence of the transition dipole matrix elements, the total excitation rate to the $D\ ^1\Pi_u^+$ and $D\ ^1\Pi_u^-$ states should be equal when the temperature is sufficiently high. When the temperature is not high enough, the total excitation rate to the $D\ ^1\Pi_u^-$ state is equal to that to the $D\ ^1\Pi_u^+$ state minus the rate due to the R(0) excitation. For the Σ–Π transition, the oscillator strength of $R(0)$ is twice the value of $(f_{J,J+1} + f_{J,J-1})$ with $J \geq 1$. Since the population of H_2 at $J_i = 0$ is 12.88% of the total at 300 K, the excitation cross section of the $D\ ^1\Pi_u^+$ would have been $1/(1 - 2 \times 0.1288)$ or 1.35 times that of the $D\ ^1\Pi_u^-$ state, if there were no perturbation and no rotational dependence of the transition dipole matrix elements. The excitation cross sections to the $D\ ^1\Pi_u^-$ and unpredissociated levels of the $D\ ^1\Pi_u^+$ state can be obtained from the calculated oscillator strengths to be 2.11×10^{-18} and 1.20×10^{-18} cm^2, respectively, at 100 eV and 300 K. Thus, the predissociation yield of the $D\ ^1\Pi_u$ state at 100 eV and 300 K is estimated to be 33% if the $^1\Sigma_u^+$–$^1\Pi_u^+$ perturbations and rotational dependence of the transition dipole matrix elements for the $D\ ^1\Pi_u$–$X\ ^1\Sigma_g^+$ system can be neglected. Alternatively, the predissociation yield is calculated to be 32% from the experimentally measured emission cross section of 1.1×10^{-18} and 1.8×10^{-18} cm^2 for the $D\ ^1\Pi_u^+$ and $D\ ^1\Pi_u^-$, respectively.

Similarly, from the measured emission cross sections of 5.3×10^{-19} and 1.0×10^{-19} cm^2 for the $D'\ ^1\Pi_u^-$ and $D'\ ^1\Pi_u^+$ state, we can estimate the nonradiative yield of the $D'\ ^1\Pi_u$ state to be ~49% at 300 K and 100 eV. However, the presence of the autoionization for the $v_j \geq 4$ levels makes the estimation less reliable. In addition, the experimental study of Namioka (1964) has suggested the presence of the perturbation between the $v_j = 0$ level of the $D'\ ^1\Pi_u^+$ state and the $v_j = 5$ and 6 levels of the $B'\ ^1\Sigma_u^+$ state. Finally, because of the weak $D'\ ^1\Pi_u$–$X\ ^1\Sigma_g^+$ transition, both emission cross sections and nonradiative yield of the $D'\ ^1\Pi_u$ state are expected to have fairly large uncertainties.

Table 2 summarizes the electronic cross sections and nonradiative yields of H_2 $np\sigma\ \Sigma_u^+\ 1$ and $np\pi\ ^1\Pi_u$ series.

5. DISCUSSION

Figure 1 shows that the emission intensities of the $B\ ^1\Sigma_u^+$–$X\ ^1\Sigma_g^+$ and $C\ ^1\Pi_u$–$X\ ^1\Sigma_g^+$ band systems are about 5 times stronger than those of the $B'\ ^1\Sigma_u^+$–$X\ ^1\Sigma_g^+$ and $D\ ^1\Pi_u$–$X\ ^1\Sigma_g^+$ band system in the wavelength region longer than 945 Å. The instrumental calibration in this region is primarily determined by the Lyman and Werner band intensities. The error in calibrated relative intensity should, in general, be less than 10% in the region from 945 Å to 1200 Å. The "strong" emissions from the $v_j = 0$ and 1 levels of the $B'\ ^1\Sigma_u^+$ state in the region are the (0, 2) band between 976 and 982 Å, (0, 3) band between 1012 and 1018 Å, (1, 4) band between 1029 and 1035 Å, and (1, 5) band between 1064 and 1070 Å regions. All the model intensities of these $B'\ ^1\Sigma_u^+$–$X\ ^1\Sigma_g^+$ transitions in the regions are 20%–30% weaker than the experimental intensities.

It is not clear what causes difference between the calculated and observed intensities for the $v_j = 0$ and 1 levels of the $B'\ ^1\Sigma_u^+$ state. The excitation function of the $B'\ ^1\Sigma_u^+$–$X\ ^1\Sigma_g^+$ band system is not expected to differ from those of the $B\ ^1\Sigma_u^+$–$X\ ^1\Sigma_g^+$ and $C\ ^1\Pi_u$–$X\ ^1\Sigma_g^+$ band systems by more than 5% at 100 eV. So, the difference cannot be due to the utilization of the Lyman and Werner band excitation function for the $B'\ ^1\Sigma_u^+$–$X\ ^1\Sigma_g^+$ band system. Perturbations by the $D\ ^1\Pi_u^+$ or higher Rydberg states are also not expected to produce the observed 20%–30% differences. The $v_j = 0$ level of the $B'\ ^1\Sigma_u^+$ state, which lies ~2400 cm^{-1} below the $v_j = 0$ level of the $D\ ^1\Pi_u^+$ state, cannot be efficiently perturbed by the $D\ ^1\Pi_u^+$ state. The $v_j = 1$ level of the $B'\ ^1\Sigma_u^+$ state is known to couple with the $v_j = 0$ level of the $D\ ^1\Pi_u^+$ state. However, couplings between the two levels cannot explain the difference between the observed and calculated intensities because the disagreement also occurs in $P(1)$ transitions, which are free from the couplings. Moreover, the calculation of Abgrall et al. (1994) should, at least partially, take into account the effect of the $B'\ ^1\Sigma_u^+$–$D\ ^1\Pi_u^+$ couplings. Perturbations of the $v_j = 0$ and 1 levels of the $B'\ ^1\Sigma_u^+$ state by higher Rydberg levels are also unlikely since the nearest level, $v_j = 0$ of the $B''\ ^1\Sigma_u^+$ state, is more than 4500 cm^{-1} away. A possible explanation for the relative intensity differences is the inaccuracy of the $B'\ ^1\Sigma_u^+$–$X\ ^1\Sigma_g^+$ transition moment. This explanation, however, can essentially be ruled out since a more recent calculation by Abgrall et al. (2000) has shown that, for the strong transitions, the new $B'\ ^1\Sigma_u^+$–$X\ ^1\Sigma_g^+$ transition probabilities differ by less than 5% from those obtained by Abgrall et al. (1994). Another explanation is that the emission intensity arising from the higher ($n \geq 4$) Rydberg states, which are not considered by the model, are not completely negligible in the 976–982 Å, 1012–1018 Å, 1029–1035 Å, and 1064–1070 Å regions. Indeed, some of the transitions involving these $n \geq 4$ Rydberg states have been identified in Figure 3. However, the explanation by $n \geq 4$ Rydberg states, even if correct, cannot account for all the differences in these four wavelength regions. Clearly, more experimental and theoretical studies are needed to remove the discrepancies between the observed and synthetic spectra.

It is interesting to compare excitation cross sections of the $B'\ ^1\Sigma_u^+$ and $D\ ^1\Pi_u$ states with those of the $B\ ^1\Sigma_u^+$ and $C\ ^1\Pi_u$ states. The $B\ ^1\Sigma_u^+$ and $C\ ^1\Pi_u$ cross sections listed in Table 2 are obtained by Liu et al. (1998) from the measured excitation function and calculated oscillator strength of Abgrall et al. (1993a, 1993b, 1993c). The effects of perturbations and rotational dependence of the transition dipole matrix elements on the cross section are fully considered. The excitation cross sections of the $B'\ ^1\Sigma_u^+$ and $D\ ^1\Pi_u$ states, however, are obtained essentially without consideration of local perturbations and rotational dependence of transition dipole matrix elements. To make a fair comparison, we need to convert the $B\ ^1\Sigma_u^+$ and $C\ ^1\Pi_u$ cross sections in Table 2 into hypothetical values when perturbations and J-dependence of the transition dipole matrix elements are

[5] Here we have implicitly excluded the high J_j levels of $v_j = 0$, 1 and 2 of the $D\ ^1\Pi_u^+$ state, which lie above the H(1s)+H(2ℓ) dissociation limit. At $T = 300$ K, excitations into these levels are completely negligible.

absent. Using the procedure outlined in § 4.4.2, we have $\sigma^0(C\ ^1\Pi_u) = 2.35 \times \sigma(C\ ^1\Pi_u^-)$. The excitation cross section for the $C\ ^1\Pi_u^-$ level at 300 K and 100 eV can be obtained as 113×10^{-19} cm^2 from the work of Liu et al. (1998). The hypothetical cross section for the $C\ ^1\Pi_u$ state is therefore $\sigma^0(C\ ^1\Pi_u) = 265 \times 10^{-19}$ cm^2. The difference, 24×10^{-19} cm^2, between the $\sigma^0(C\ ^1\Pi_u)$ and $\sigma(C\ ^1\Pi_u)$ represents the cross section transfer from the $C\ ^1\Pi_u^+$ state into the $B\ ^1\Sigma_u^+$ state. The hypothetical cross section of the $B\ ^1\Sigma_u^+$ state is thus $\sigma^0(B\ ^1\Sigma_u^+) = 238 \times 10^{-19}$ cm^2. We note that $\sigma^0(C\ ^1\Pi_u)$ is about 11% larger than $\sigma^0(B\ ^1\Sigma_u^+)$. Likewise, the estimated cross section of the $D\ ^1\Pi_u$ is about 5% greater than its counterpart. Moreover, the excitation cross sections of the $np\sigma\ ^1\Sigma_u^+$ and $np\pi\ ^1\Pi_u$ series decrease by 82% and 83%, respectively, as the n increases from 2 to 3.

For a pure Rydberg series, the excitation cross section should fall according to $(n - \delta)^3$, where δ is the quantum defect which arises from the nonspherical symmetry of H_2 and deviation from the pure Coulomb field due to the finite size of the charge distribution. The quantum defect of the $B\ ^1\Sigma_u^+$, $C\ ^1\Pi_u$, $B'\ ^1\Sigma_u^+$, and $D\ ^1\Pi_u$ states can be estimated from their lowest observed level energy. Using IP = 124,417.507 cm^{-1} (Gilligan & Eyler 1992) and R_H = 109,677.576 cm^{-1}, we find that the quantum defects for the $B\ ^1\Sigma_u^+$, $C\ ^1\Pi_u$, $B'\ ^1\Sigma_u^+$, and $D\ ^1\Pi_u$ states are 0.21, −0.08, 0.19, and −0.09, respectively. The value of quantum defect suggests cross section ratios of 3.9 and 3.3 for $\sigma^0(B\ ^1\Sigma_u^+)/\sigma^0(B'\ ^1\Sigma_u^+)$ and $\sigma^0(C\ ^1\Pi_u)/\ \sigma^0(D\ ^1\Pi_u)$, respectively. The cross section ratios obtained in the present work, however, are 5.5 and 5.9, respectively. The differences are significantly larger than the expected experimental errors and indicate that the simple scaling formula does not work very well for the low-n states.

The predissociation of the $D\ ^1\Pi_u^+$ state has been studied by Julienne (1971), Fiquet-Fayard & Gallais (1972), and Glass-Maujean et al. (1978, 1979). In the experimental work of Glass-Maujean et al. (1978), absorption and atomic hydrogen fragment Lyα emission spectra were recorded simultaneously. The $D\ ^1\Pi_u^+$ state was found to predissociate fully from the $v_j = 3$ level to the ionization limit. Moreover, the lifetimes of $J_j = 2$ of the $v_j = 3$–11 levels were determined to be $(3.7–5.9) \times 10^{-13}$ s from the line width. In addition to the coupling with the continuum levels of the $B'\ ^1\Sigma_u^+$ state, Glass-Maujean et al. (1979) also suggested that the coupling between the $D\ ^1\Pi_u^+$ and $B''\ ^1\Sigma_u^+$ states might be another predissociation channel for the $v_j = 10$ and 11 levels of $D\ ^1\Pi_u^+$ state. The radiative lifetimes of the $D\ ^1\Pi_u^-$ state and $v_j = 0$, 1, and 2 levels of the $D\ ^1\Pi_u^+$ are calculated to be in the range of 2.3×10^{-9} to 3.3×10^{-9} s (Abgrall et al. 1994). The emission branching-ratio for the $J_j = 2$ and $v_j = 3$–11 levels of the $D\ ^1\Pi_u^+$ state is, at most, 0.02%. Hence, the $v_j \geq 3$ levels can indeed be considered to predissociate completely.

The relation between the excitation cross sections of the Π^+ and Π^- components, $\sigma(\Pi^+)(1–2\ N_{J=1}/N_t) = \sigma(\Pi^-)$, of § 4.4.2 are obtained with assumptions that (1) the effect due to the difference in threshold energy is negligible; (2) the sum of the $P(J)$ and $R(J)$ branch oscillator strengths ( ) is independent of rotational quantum numbers; and (3) the sum the P(J) and R(J) branch oscillator strengths, $(f_{J,J+1} + f_{J,J-1})$, is equal to that of the $Q(J)$ branch, $f_{J,J}$. As all threshold energies of H_2 excitation fall between 10.5 and 14.5 eV, the first assumption is unlikely to introduce any significant errors if the excitation energy is above 30 eV. However, the presence of local or accidental perturbations and significant rotational dependence of the Frank-Condon factor, particularly for the vibrational bands that carry large absorption oscillator strength, will invalidate the second and third assumptions. For example, on the basis of $\sigma(C\ ^1\Pi_u^-) = 113 \times 10^{-19}$ cm^2 and $\sigma(C\ ^1\Pi_u^+) = 128 \times 10^{-19}$ cm^2, the relation would erroneously suggest a dissociation yield of ∼9% for the $C\ ^1\Pi_u$ state, when actually the local perturbations between $v = 12$ and 14 of the $B\ ^1\Sigma_u^+$ and $v = 2$ and 3 of the $C\ ^1\Pi_u^+$ are primarily responsible for the deviation. Moreover, as the principal quantum number increases, the energy separation between the $np\sigma\ ^1\Sigma_u^+$ and $np\pi\ ^1\Pi_u$ states decreases and the coupling between the $np\sigma\ ^1\Sigma_u^+$ and $np\pi\ ^1\Pi_u^+$ increases. For large n, the energy gaps between the $np\sigma\ ^1\Sigma_u^+$ and $np\pi\ ^1\Pi_u$ Rydberg series are no longer observed, and the rotational levels are solely arranged on the basis of the rotational levels of the H_2^+ core to which the series converge (i.e., Hund's case d). Under these circumstances, the $np\sigma\ ^1\Sigma_u^+$ and $np\pi\ ^1\Pi_u^+$ states are strongly mixed and $np\pi\ ^1\Pi_u^+$ and $np\pi\ ^1\Pi_u^-$ can no longer be viewed as degenerate. According to the works of Herzberg & Jungen (1972) and Dehmer & Chupka (1976), the transition from case b to case d occurs at about $n = 8$ for H_2. Thus, the cross section relation between $\sigma(\Pi^+)$ and $\sigma(\Pi^-)$ is expected to totally break down when $n \geq 8$.

The predissociation yield of the $D\ ^1\Pi_u$ state in Table 2 is obtained by utilization of the cross section relation between the Π^+ and Π^- components, which assumes the absence of the $^1\Sigma_u^+$ and $^1\Pi_u^+$ coupling. However, since the predissociation of the $D\ ^1\Pi_u^+$ state is a consequence of the coupling between the $v_j \geq 3$ level of the $D\ ^1\Pi_u^+$ and the continuum levels of the $B'\ ^1\Sigma_u^+$ state, the effect of the coupling on the excitation cross section and predissociation yield also need to be addressed. In general, a coupling between two states results in a mixture of two wave functions and, therefore, repartitioning of absorption oscillator strengths. However, the sum of the oscillator strength over the two coupled states does not change. The sum of the two excitation cross sections is likewise not affected by the couplings. The cross sections of the $D\ ^1\Pi_u^+$ and continuum levels of the $B'\ ^1\Sigma_u^+$ state in the absence of coupling can be estimated. For instance, the cross section for the continuum levels of the B′ $^1\Sigma_u^+$ state has been estimated to be 1.6×10^{-18} cm^2 on the basis of the calculated total continuum and discrete oscillator strength of the $P(1)$ transitions, which are free from $D\ ^1\Pi_u^+$–$B'\ ^1\Sigma_u^+$ couplings. The cross section of the $D\ ^1\Pi_u^+$ state is 1.35 times that of $D\ ^1\Pi_u^-$, or 2.3×10^{-18} cm^2, based on the measured $D\ ^1\Pi_u^-$ cross section, which is also free from perturbation. The sum of the cross sections for the $D\ ^1\Pi_u^+$ levels below the H(1s)+H(2ℓ) limit (i.e., $v_j = 0$, 1, and 2) are measured or calculated to be 1.1×10^{-18} cm^2. Thus, the cross section for the $D\ ^1\Pi_u^+$ levels above the limit is 1.2×10^{-18} cm^2. Since the cross sections for the $v_j \geq 3$ levels of the $D\ ^1\Pi_u^+$ state and the continuum levels of the $B'\ ^1\Sigma_u^+$ state are similar (1.2×10^{-18} vs. 1.6×10^{-18}), the $B'\ ^1\Sigma_u^+$–$D\ ^1\Pi_u^+$ coupling, while responsible for the predissociation of the $D\ ^1\Pi_u^+$ state, does not have a significant effect on the magnitude of the cross section of the $D\ ^1\Pi_u^+$ state and continuum levels of the $B'\ ^1\Sigma_u^+$ state. For example, in the extreme case of 50%/50% mixing ratio, cross sections for the $v_j \geq 3$ levels of the $D\ ^1\Pi_u^+$ state and the continuum levels of the $B'\ ^1\Sigma_u^+$ state both become 1.4×10^{-18} cm^2. The total cross sections for the $B'\ ^1\Sigma_u^+$ and $D\ ^1\Pi_u$ states change from 3.8×10^{-18} and 4.0×10^{-18} to 3.6×10^{-18} and 4.2×10^{-18} cm^2, respectively. The dissociation and

predissociation yield for the $B'\ ^1\Sigma_u^+$ and $D\ ^1\Pi_u$ state vary from 44% and 30% to 39% and 33%, respectively. All these variations due to the coupling are within the experimental error.

The predissociation of the $D'\ ^1\Pi_u^+$ state has been studied by Guyon et al. (1979), Glass-Maujean et al. (1978, 1987), and Glass-Maujean (1979). Except for the $v_j = 0$ level, which lies below the H(1s) + H(2ℓ) limit, all other v_j levels of the $D'\ ^1\Pi_u^+$ state are predissociated by indirect couplings with the $B'\ ^1\Sigma_u^+$ continuum levels. There are two coupling mechanisms for the $D'\ ^1\Pi_u^+$ state: Coriolis coupling with the $B''\ ^1\Sigma_u^+$ levels that are predissociated by homogeneous coupling with the continuum levels of the $B'\ ^1\Sigma_u^+$ state and homogeneous coupling with the $D\ ^1\Pi_u^+$ levels that are predissociated by Coriolis coupling with the $B'\ ^1\Sigma_u^+$ continuum levels. Glass-Maujean (1979) has shown that the two predissociation mechanisms are of opposite sign and their contributions to the predissociation of the $D'\ ^1\Pi_u^+$ destructively interfere with each other. For the $v_j \geq 4$ levels, the autoionization also takes place (Dehmer & Chupka 1976), although there are some disagreements on the magnitude of autoionization probabilities (Glass-Maujean 1979). The predissociation yields for the $J_j = 1$–4 of the $v_j = 1$–7 levels of the $D'\ ^1\Pi_u^+$ state have been found to range from 60% to 95% with uncertainties of 5%–20% (Glass-Maujean et al. 1987). With consideration of autoionization, emission branching ratios of the $v_j \geq 1$ levels of the $D'\ ^1\Pi_u^+$ state are indeed very small. In fact, emissions from these levels are too weak to be measured accurately in the present study. We note that the yield of nonradiative process for the $D'\ ^1\Pi_u^+$ state (86%) obtained in the present work is consistent with predissociation yield and autoionization yields obtained by Dehmer & Chupka (1976), Guyon et al. (1979), Glass-Maujean (1979), and Glass-Maujean et al. (1987).

When one compares the cross sections obtained in the present work and with those of Ajello et al. (1988) in Table 2, the previous cross sections are, in general, significantly larger than the present ones. For example, the previous emission cross sections for $B'\ ^1\Sigma_u^+$, $D\ ^1\Pi_u$, and $D'\ ^1\Pi_u$ are larger than the present ones by factors of 3.4, 1.5, and 3.0, respectively. These large differences between the two sets of the data are due to low spectral resolution ($\sim$5 vs. 0.115 Å), utilization of inaccurate transition probabilities and neglecting of the $^1\Sigma_u^+$ and $^1\Pi_u^+$ perturbation in the previous work. Since the predissociation yield is derived from excitation and emission cross sections, the large errors in the emission cross sections of Ajello et al. (1988) also suggest a serious error in their predissociation yields.

The $B\ ^1\Sigma_u^+$ and $C\ ^1\Pi_u$ cross sections of Ajello et al. (1988) are based on the experimental work of Shemansky et al. (1985a) and oscillator strengths of Allison & Dalgarno (1970). Since the Allison-Dalgarno oscillation strengths are obtained without consideration of rotational motion, it is interesting to compare the Shemansky et al. (1985a) $B\ ^1\Sigma_u^+$ and $C\ ^1\Pi_u$ cross sections with the "perturbation-free" cross sections for $B\ ^1\Sigma_u^+$ (238×10^{-19} cm^2) and $C\ ^1\Pi_u$ (265×10^{-19} cm^2) obtained in the present work. The differences between the two sets of cross sections are 12% and 5% for the $B\ ^1\Sigma_u^+$ and $C\ ^1\Pi_u$ states, respectively. These difference do not at first appear to be consistent. However, it should be remembered that the previous $B\ ^1\Sigma_u^+$ and $C\ ^1\Pi_u$ cross sections have been reduced by 8% and 14%. If the reduction, which has been shown to be incorrect by the calculation of Dressler & Wolniewicz (1985), is removed, the differences between the "perturbation-free" and restored previous $B\ ^1\Sigma_u^+$ and $C\ ^1\Pi_u$ cross sections are 20% and 19%, respectively. As explained in the work of Liu et al. (1998), the difference is caused by the inaccurate excitation functions of Shemansky et al.

6. CONCLUSION

High-resolution EUV emission spectra of molecular hydrogen have been obtained in the wavelength range 800–1440 Å. Application of a synthetic spectrum using the $B\ ^1\Sigma_u^+$–$X\ ^1\Sigma_g^+$, $C\ ^1\Pi_u$–$X\ ^1\Sigma_g^+$, $B'\ ^1\Sigma_u^+$–$X\ ^1\Sigma_g^+$, and $D\ ^1\Pi_u$–$X\ ^1\Sigma_g^+$ transition probabilities calculated by Abgrall et al. (1993a, 1993b, 1993c, 1994) permits an instrumental sensitivity calibration and measurement of emission cross sections of the $B'\ ^1\Sigma_u^+$, $D\ ^1\Pi_u$, $B''\ ^1\Sigma_u^+$, $D'\ ^1\Pi_u$, and $D''\ ^1\Pi_u$ states. Spectral analysis shows that the synthetic spectra accurately reproduce observed intensities for $B\ ^1\Sigma_u^+$–$X\ ^1\Sigma_g^+$, $C\ ^1\Pi_u$–$X\ ^1\Sigma_g^+$, and $D\ ^1\Pi_u$–$X\ ^1\Sigma_g^+$ transitions. However, significant discrepancies for a few vibrational bands of the $B'\ ^1\Sigma_u^+$–$X\ ^1\Sigma_g^+$ transition also exist.

The research described in this paper was carried out at the Jet Propulsion Laboratory and University of Southern California and was sponsored by the US Air Force Office of Scientific Research (AFOSR), the Aeronomy Program of the National Science foundation (ATM 93-20589) and the NASA Planetary Atmospheres Program Office, and the NASA Space Astrophysics Research and Analysis Program. One of us (C. J.) is supported by the National Research Council through a Resident Research Associateship at the Jet Propulsion Laboratory. We particularly thank R. Keski-Kuha and J. Gum of the NASA Goddard Spaceflight Center for performing the boron carbide grating coating used in this experiment. We would also like to acknowledge the contribution of E. Roueff in the previous work.

REFERENCES

Abgrall, H., Launay, F., Roueff, E., & Roncin, J. Y. 1987, J. Chem. Phys., 87, 2036
Abgrall, H., & Roueff, E. 1989, A&AS, 79, 313
Abgrall, H., Roueff, E., & Drira I. 2000, A&AS, 141, 297
Abgrall, H., Roueff, E., Launay, F., & Roncin, J. Y. 1994, Canadian J. Phys., 72, 856
Abgrall, H., Roueff, E., Launay, F., Roncin, J. Y., & Subtil, J. L. 1993a, A&AS, 101, 273
———. 1993b, A&AS, 101, 323
———. 1993c, J. Mol. Spectrosc., 157, 512
Abgrall, H., Roueff, E., Liu, X., & Shemansky, D. E. 1997, ApJ, 481, 557
Abgrall, H., Roueff, E., Liu, X., Shemansky, D. E., & James, G. K. 1999, J. Phys. B, 32, 3813
Ajello, J. M., Shemansky, D. E., Kwok, T. L., & Yung, Y. L. 1984, Phys. Rev. A, 29, 636
Ajello, J. M., et al. 1988, Appl. Opt., 27, 890
Ajello, J. M., et al. 1998, J. Geophys. Res., 103, 20,125
Allison, A. C., & Dalgarno, A. 1970, At. Data Nucl. Data Tables, 1, 289
Balakrishnam, A., Smith, V., & Stoicheff, B. P. 1992, Phys. Rev. Lett., 68, 2149
———. 1994, Phys. Rev. A, 49, 2460
Bardsley, J. N. 1967, Chem. Phys. Lett., 1, 229
Berry, R. S. 1966, J. Chem. Phys., 45, 1228
Beswick, J. A., & Glass-Maujean, M. 1987, Phys. Rev. A, 35, 3359
Broadfoot, A. L., et al. 1979, Science, 204, 709
Chupka, W. A. 1987, J. Chem. Phys., 87, 1488
Clarke, J. T., Jaffel, L. B., Vidal-Madjar, A., Gladstone, G. R., Waite, J. H., Jr., Prangé, R., Gérard, J.-C., & Ajello, J. M. 1994, ApJ, 430, L73
Clarke, J. T., Moos, H. W., Atreya, S. K., & Lane, A. L. 1980, ApJ, 241, 179
Cornaggia, C., Giusti-Suzor, A., & Jungen, Ch. 1987, J. Chem. Phys., 87, 3934
Cravens, T. E., & Dalgarno, A. 1978, ApJ, 219, 750

Dehmer, P. M., & Chupka, W. A. 1976, J. Chem. Phys., 65, 2243
———. 1995, J. Phys. Chem., 99, 1686
Dehmer, J. L., Dehmer, P. M., West, J. B., Hayes, M. A., Siggel, M. R. F., & Parr, A. C. 1992, J. Chem. Phys., 97, 7911
Dressler, K., & Wolniewicz, L. 1985, J. Chem. Phys., 82, 4720
———. 1986, J. Chem. Phys., 85, 2821
Drira, I. 1999, J. Mol. Spectrosc., 52, 198
Fiquet-Fayard, F., & Gallais, O. 1972, Chem. Phys. Lett., 16, 18
Ford, A. L., Brown, J. C., Shipsey E. J., & DeVries P. 1975, J. Chem. Phys., 63, 362
Gilligan, J. M., & Eyler, E. E. 1992, Phys. Rev. A, 46, 3676
Glab, W. L., & Hessler, J. P. 1987, Phys. Rev. A, 35, 2102
———. 1990, Phys. Rev. A, 42, 5486
Glass-Maujean, M. 1979, Chem. Phys. Lett., 68, 320
———. 1984, At. Data Nucl. Data Tables, 30, 301
Glass-Maujean, M., Breton, J., & Guyon, P. M. 1978, Phys. Rev. Lett., 40, 181
———. 1979, Chem. Phys. Lett., 63, 591
———. 1987, Zs. Phys. D, 5, 189
———. 1985a, J. Chem. Phys., 83, 1468
Glass-Maujean, M., Breton, J., Thieblemont, B., & Ito, K. 1985b, Phys. Rev. A, 32, 947
Glass-Maujean, M., Frohlich, H., & Beswick, J. A. 1988, Phys. Rev. Lett., 61, 157
Gredel, R., Lepp, S., Dalgarno, A., & Herbst, E. 1989, ApJ, 347, 289
Guyon, P. M., Breton, J., & Glass-Maujean, M. 1979, Chem. Phys. Lett., 68, 314
Herzberg, G., & Jungen, Ch. 1972, J. Mol. Spectrosc., 41, 425
Hinnen, P. C., Hogervorst, W., Stolte, S., & Ubachs, W. 1994a, Appl. Phys. B, 59, 307
———. 1994b, Canadian J. Phys., 72, 1032
Hinnen, P. C., & Ubachs, W. 1995, Chem. Phys. Lett., 240, 351
———. 1996, Chem. Phys. Lett., 254, 32
Hinnen, P. C., Werners, S. E., Stolte, S., Hogervorst, W., & Ubachs, W. 1995, Phys. Rev. A, 52, 4425
Hogervorst, W., Eikema, K. S. E., Reinhold, E., & Ubachs, W. 1998, Nucl. Phys. A, 631, C353
Huber, K. P., & Herzberg, G. 1979, Molecular Spectra & Molecular Structure: IV, Constants of Diatomic Molecule (New York: Van Nostrand)
Julienne, P. J. 1971, Chem. Phys. Lett., 8, 27
Jungen, Ch. 1984, Phys. Rev. Lett., 53, 2394
Jungen, Ch., & Atabek, O. 1977, J. Chem. Phys., 66, 5584
Kim, Y. H., Caldwell, J. J., & Fox, J. L. 1995, ApJ, 447, 906
Liu, X., Ahmed, S. M., Multari, R. A., James, G. K., & Ajello, J. M. 1995, ApJS, 101, 375
Liu, X., Shemansky, D. E., Ahmed, S. M., James, G. K., & Ajello, J. M. 1998, J. Geophys. Res., 103, 26,739
Liu, X., Shemansky, D. E., Ajello, J. M., Hansen, D. L., Jonin, C., & James, G. K. 2000, ApJS, 129, 267 (Paper II)
McCormack, E. F., Pratt, S. T., Dehmer, P. M., & Dehmer, J. L. 1993, J. Chem. Phys., 98, 8370
Monfils, A. 1961, Acad. Roy. Belg. Bull., Cl. Sci., 47, 816
Morrissey, P. F., Feldman, P. D., Clarke, J. T., Wolven, B. C., Strobel, D. F., Durrance, S. T., & Trauger, J. T. 1997, ApJ, 576, 918
Mulliken, R. S. 1966, J. Am. Chem. Soc., 88, 1849
Namioka, T. 1964, J. Chem. Phys., 41, 2141
Pratt, S. T., Dehmer, J. L., Dehmer, P. M., & Chupka, W. A. 1992, J. Chem. Phys., 97, 3038
———. 1994, J. Chem. Phys., 101, 882
Pratt, S. T., McCormack, E. F., Dehmer, J. L., Dehmer, P. M., & Chupka, W. A. 1990, J. Chem. Phys., 92, 1831
Raolut, M., & Jungen, Ch.1981, J. Chem. Phys., 74, 3388
Raymond, J. C., Blair, W. P., & Long, K. S. 1997, ApJ, 489, 314
Reinhold, E., Hogervorst, W., & Ubachs, W. 1996, J. Mol. Spectrosc., 180, 156
———. 1997, Phys. Rev. Lett., 78, 2543
Roncin, J. Y., & Launay, F. 1994, Atlas of the Vacuum Ultraviolet Emission Spectrum of Molecular Hydrogen (Wordbury, NY: AIP)
Rothenberg, S., & Davidson, E. R. 1967, J. Mol. Spectrosc., 22, 1
Senn, P., Quadrelli, P., & Dressler, K. 1988, J. Chem. Phys., 89, 7401
Shemansky, D. E., Ajello, J. M., & Hall, D. T. 1985a, ApJ, 296, 765
Shemansky, D. E., Ajello, J. M., Hall, D. T., & Franklin, B. 1985b, ApJ, 296, 774
Shull, J. M., & Beckwith, S. 1982, ARA&A, 20, 163
Stephens, T., & Dalgarno, A. 1972, J. Quant. Spectrosc. Radiat. Transfer, 12, 569
Sternberg, A., Dalgarno, A., & Lepp, S. 1987, ApJ, 320, 676
Takezawa, S. 1970, J. Chem. Phys., 52, 2575
Trafton, L. M., Gérard, J. C., Munhoven, G., & Waite, J. H., Jr. 1994, ApJ, 421, 816
Ubachs, W., Hinnen, P. C., & Reinhold, E. 1997, ApJ, 476, L93
Wolniewicz, L. 1969, J. Chem. Phys., 51, 5002
———. 1995, Chem. Phys. Lett., 233, 644
Wolniewicz, L., & Dressler, K. 1988, J. Chem. Phys., 88, 3861
———. 1992, J. Chem. Phys., 96, 6053